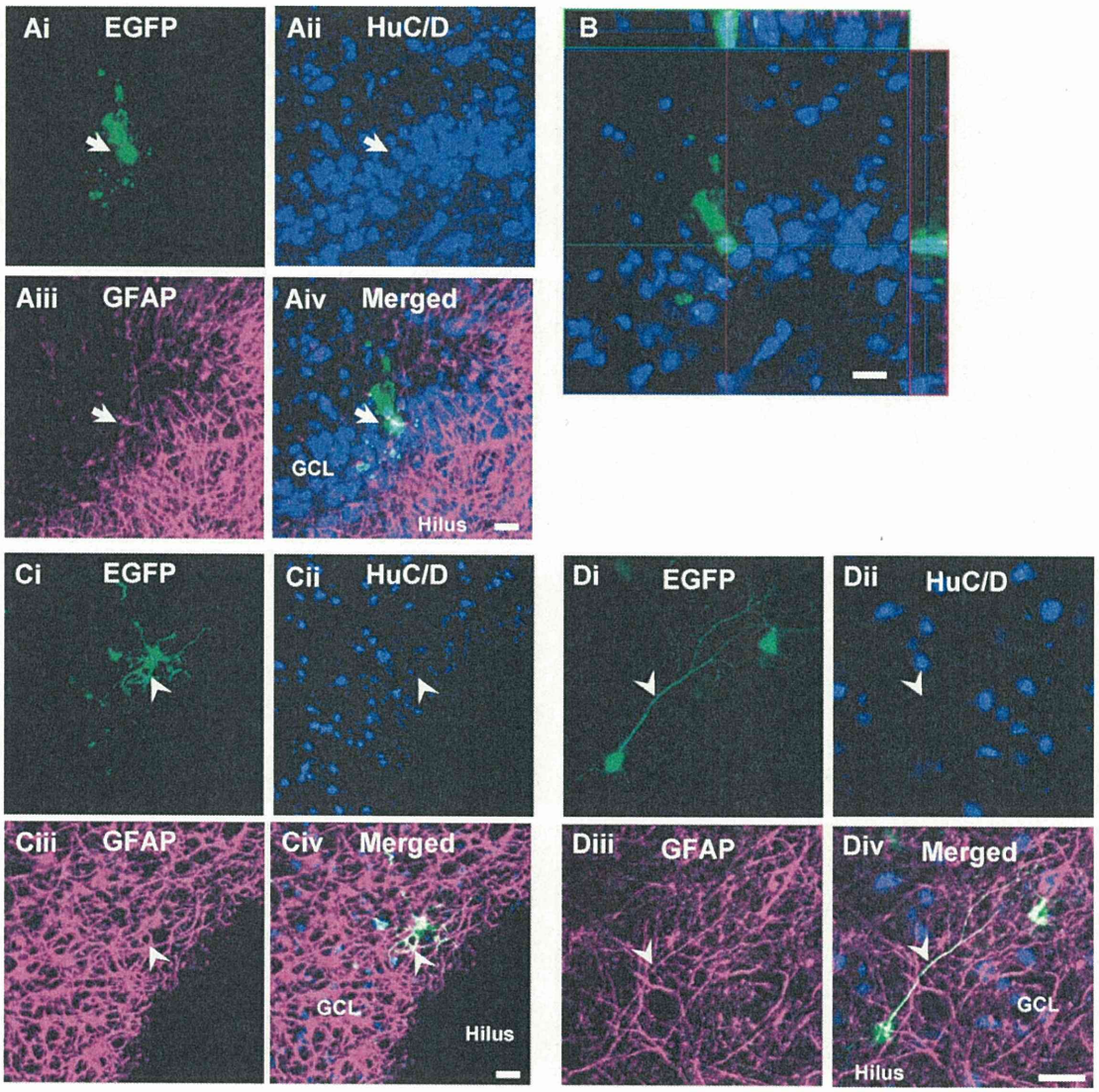

Fig. 3. Phenotype determination of the lineages. (A) A HuC/D-positive lineage cell. The phenotype of one of the EGFP-expressing cells (Ai, arrow) was examined immunohistochemically by using either anti-HuC/D antibody (Aii) or anti-GFAP antibody (Aiii). The merged image indicates that this cell is positive for HuC/D but negative for GFAP (Aiv). (B) Three-dimensional analysis of the cell shown in (A). (C) Similar to Ai–iv but the GFAP-positive lineage cell with an astrocyte-like appearance. (D) Another GFAP-positive lineage cell with a radial glia-like appearance. Scale bars, 20 μm.

Among all 87 lineages examined, 30 lineages (34%) were HuC/D-positive (Supplementary Fig. S3) and 15 lineages (17%) were GFAP-positive (Supplementary Fig. S4). When one of the descendent cells was HuC/D-positive, no GFAP-positive cells were generated in the same lineage as we examined. However, pair of "unclassified" cells was generated in one lineage. When one of the descendent cells was GFAP-positive, other members in the same lineage were also GFAP-positive. Again, no HuC/D-positive cells were found in any GFAP-positive lineage as we examined. The remaining lineages were unclassified as all the descendents became untraceable before 28 DPI ($n = 21$, 24%), or they were neither HuC/D- nor GFAP-positive ($n = 21$, 25%) (Supplementary Fig. S5). These lineages were not included in the following numerical analyses.

3.2. Quantitative analysis of the lineages

Among the HuC/D-positive lineages, 10/30 lineages showed no further proliferation, 10/30 divided once after EGFP expression and 10/30 divided more than twice. The EGFP-expressing cells were occasionally detectable as pairs opposite to each other (dividing pairs) (Kamada et al., 2004). As a result, 63 cells were finally produced. However, 23/63 cells were untraceable shortly after division in the searching field whereas others were traceable as long as up to 28 DPI. On the other hand, in the GFAP-positive lineage, the newly generated cells were rarely untraceable.

The frequency of cell division was summarized for both the HuC/D-positive (Fig. 4A) and the GFAP-positive groups (Fig. 4B) in each 1–7, 8–14, 15–21 or 22–28 DPI period. In both groups of lineages, the frequency was higher during the early DPI period (1–7 and 7–14) than the later (15–21 and 22–28 DPI) with significant differences ($P < 0.05$, One-way ANOVA with post hoc Scheffe's F-test). As shown in Fig. 4C, the proliferation of HuC/D-positive lineage cells was significantly less than expected from the predicted value ($P < 0.05$, One-sample Wilcoxon signed rank test). This is in contrast to that of GFAP-positive lineage cells, which was almost identical to the prediction (Fig. 4D). This difference could be attributed to the presence of large numbers of untraceable cells after cell division in the HuC/D-positive lineages. As summarized in Fig. 4E, the survival probability was 0.73 ± 0.05 ($n = 30$) in the HuC/D-positive lineages,

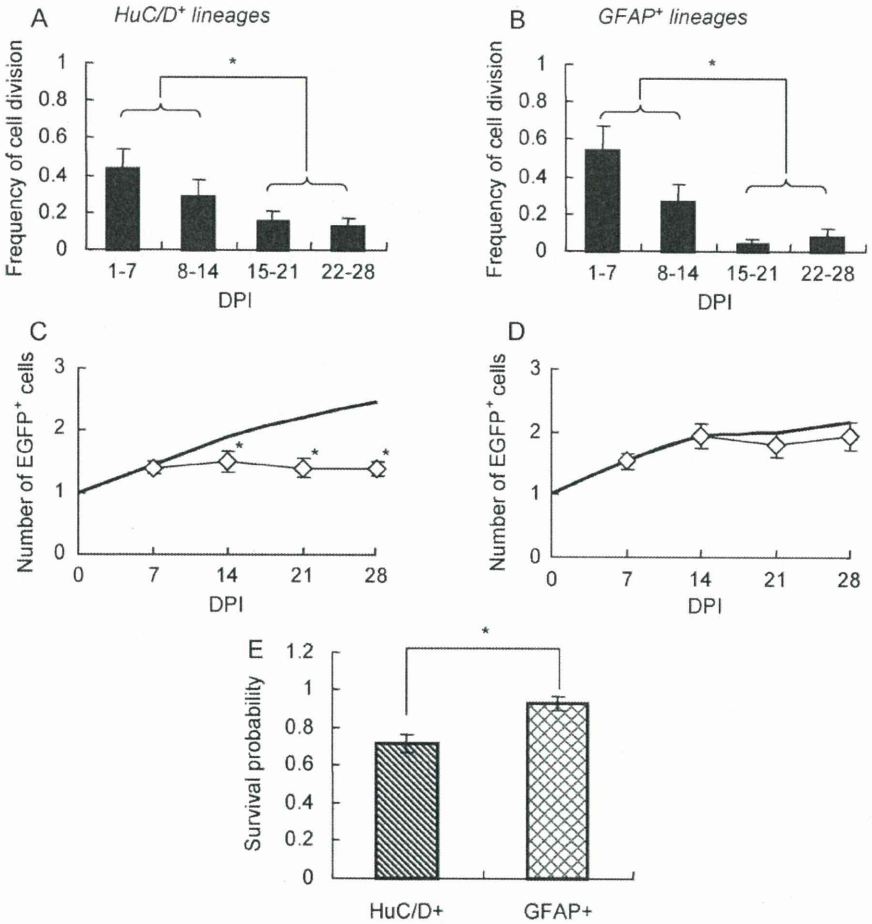

Fig. 4. Proliferation of newborn cells. A and C from the HuC/D-positive lineages ($n = 30$) and B and D from the GFAP-positive lineages ($n = 15$). (A, B) The frequency of cell division during each of the four period 1–7, 8–14, 15–21 and 22–28 DPI (mean ± SEM). The difference was statistically examined (One-way ANOVA with post hoc Scheffe's *F*-test) between the early DPI period (1–7 and 7–14) and the later (15–21 and 22–28 DPI). $^*P < 0.05$. (C, D) The time-dependent change of the number of EGFP-expressing cells (open symbols and bars, mean ± SEM). The thick line is the proliferation curve expected from the frequency of cell division shown in A or B. * indicates the significant difference from the prediction ($P < 0.05$, One-sample Wilcoxon signed rank test). (E) Summary of the survival probability (mean ± SEM) in the HuC/D-positive and GFAP-positive lineages. $^*P < 0.01$ (Mann–Whitney *U*-test).

which was significantly smaller than that in the GFAP-positive lineages (0.93 ± 0.05, $n = 15$; $P < 0.05$, Mann–Whitney *U*-test).

In 18/30 HuC/D-positive lineages one of the newly divided cells survived as long as 28 DPI, whereas another became untraceable. The follow-up period was distributed between 7 and 25 days with a mean of 17.9 ± 1.1 DPI ($n = 25$) (Fig. 5A). However, 11/25 cells became untraceable after the second division, 9/25 cells after the third division and 1/25 cells after the fourth division. Therefore, the postmitotic period of an untraceable cell was measured directly from the lineage tree and was summarized in Fig. 5B. It distributed between 2 and 14 days (mean, 6.5 ± 0.8 days; $n = 25$). The postmitotic period was also measured for 21 lineages in which all the descendents became untraceable before 28 DPI. Similar to that of the HuC/D-positive lineages, its distribution was between 1 and 16 days (mean, 7.7 ± 0.7 days; $n = 31$, Supplementary Fig. S6C).

3.3. Differentiation of neuron-like descendents

We also identified the phenotypes of EGFP-expressing cells immunohistochemically at 28 DPI by other markers, Prox1 and NeuN. As shown in Fig. 6Ai–iv and B, some of the Prox1- and EGFP-expressing cells were also positive for NeuN, and designated as $Prox1^+/NeuN^+$ cells. On the other hand, a significant number of the Prox1-positive cells did not express NeuN ($Prox1^+/NeuN^-$ cells) (Fig. 6Ci–iv, D). A small number of the EGFP-expressing cells (2 in 71 cells examined) were positive for NeuN, but negative for Prox1 ($Prox1^-/NeuN^+$). Among 49 lineages producing Prox1-positive cells (Supplementary Fig. S7), both NeuN-positive and NeuN-negative cells arose in 3/49 lineage. Among 23 cases of the last division in the $Prox1^+/NeuN^+$ lineages, 8 cases had two $Prox1^+/NeuN^+$ cells, 9 cases had one untraceable cell and 3 cases had two untraceable cells. In another 3 cases, one of the descendents was NeuN-negative. In both $Prox1^+/NeuN^-$ (Fig. 7A) and $Prox1^+/NeuN^+$ (Fig. 7B) lineages, the frequency of cell division was higher during the early DPI period (1–7 and 7–14) than the later (15–21 and 22–28 DPI) with significant differences ($P < 0.05$, One-way ANOVA with post hoc Scheffe's *F*-test). Newly divided cells became often untraceable in either lineage of $Prox1^+/NeuN^+$ or $Prox1^+/NeuN^-$ cells. Among 71 cells that were finally produced, 28/71 became untraceable shortly after division in the searching field whereas others were traceable as long as up to 28 DPI. Once untraceable, they never reappeared at 28 DPI under confocal microscopy with anti-EGFP immunohistochemistry even when they became untraceable only a few days before. As a result, the proliferation was significantly less than expected from the predicted value at 28 DPI in the $Prox1^+/NeuN^-$ lineage group (Fig. 7C) ($P < 0.05$, One-sample Wilcoxon signed rank test) and was significantly less than expected at 14, 21 and 28 DPI in the $Prox1^+/NeuN^+$ lineage group (Fig. 7D) ($P < 0.05$, One-sample Wilcoxon signed rank test). The postmitotic period of an untraceable cell distributed between 2 and 18 days (mean, 6.3 ± 1.5

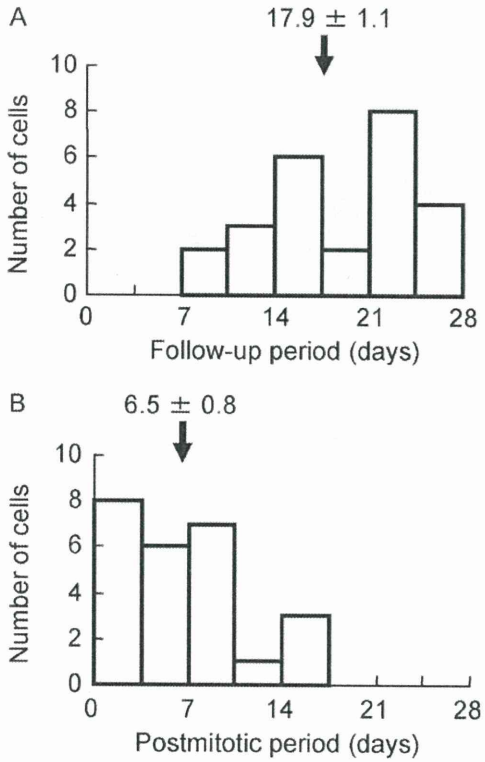

Fig. 5. Lifetime analysis. (A) Histogram of the follow-up periods in the HuC/D-positive lineages ($n=25$). (B) Histogram of the postmitotic periods of untraceable cells ($n=25$). Arrows and numbers indicate the mean (±SEM) values.

days; $n=11$) for the Prox1$^+$/NeuN$^-$ lineages (Fig. 7E), whereas it did between 2 and 10 days (mean, 5.3 ± 0.5 days; $n=22$) for the Prox1$^+$/NeuN$^+$ lineages (Fig. 7F). There was no significant difference in the postmitotic period ($P>0.9$, Kolmogorov–Smirnov test). The postmitotic period was measured also for the phenotypically identified GCL neuron. It was distributed between 3 and 26 days (mean, 15.0 ± 2.0 days; $n=44$) for the Prox1$^+$/NeuN$^-$ lineages (Fig. 7G) with insignificant difference from that of untraceable cells ($P>0.05$, Kolmogorov–Smirnov test). However, 12/25 cells survived over 23 days. For the Prox1$^+$/NeuN$^+$ lineages, as shown in Fig. 7H, it was between 12 and 28 days (mean, 20.1 ± 0.6 days; $n=44$) with negligible overlap of the postmitotic period distribution of the untraceable cells ($P<10^{-12}$, Kolmogorov–Smirnov test).

4. Discussion

In the present study, we identified newly generated cells using a retroviral labeling method in an organotypic slice culture of the hippocampus. This method enabled us to survey the lineage of a newborn cell up to 28 DPI and to determine retrospectively the phenotype of the descendent cells using the specific markers, HuC/D, GFAP, Prox1 and NeuN. In our experiments, slices were usually obtained from the dorsal part of rat hippocampus at P7, the retroviruses were inoculated restrictively in the suprapyramidal blade of GCL at 14 DIV and the fate of the EGFP-expressing cells were followed up only in the suprapyramidal region. Although it is possible that the region- or age-dependent difference of neurogenic ability is present, we did not do any systematic study on it.

4.1. The phenotypes of newly generated EGFP-expressing cells

When we identified the phenotypes of the newly generated cells at 3 DPI, we found in the GCL that 17% were positive for both nestin and GFAP and that 35% were positive for both nestin and HuC/D. Therefore, these newly divided cells consisted of both multi-potent type-1 cells which express both nestin and GFAP (Kempermann et al., 2004; Steiner et al., 2006; Roybon et al., 2009) and the neuron-destined type-2, -3 cells which express both nestin and HuC/D (Steiner et al., 2004; Seki et al., 2007). Nestin-negative and HuC/D-positive cells (17%) and a subpopulation of cells which were neither positive to nestin nor GFAP (52%) can be classified into newborn neurons. However, there remains the EGFP-expressing cells neither nestin nor HuC/D (32%) and those negative to nestin, HuC/D and GFAP (estimated to be 35%). Some of them are possibly involved in non-neuronal lineages such as proliferating astrocytes, oligodendrocytes and microglia. The pluripotent NG2 cells are possibly included in these cells (Belachew et al., 2003; Thallmair et al., 2006; Rivers et al., 2008; Zhu et al., 2008). In our slice culture, GCL neurons are clustering in the relatively thin layer under the astrocytic layer (Kamada et al., 2004). It is possible that some of these covering astrocytes are proliferating in the slice culture (Namba et al., 2005). Although the neuronal network became stabilized before 14 DIV (Buchs et al., 1993) after transient rearrangements (Robain et al., 1994; Gutierrez and Heinemann, 1999) in the slice culture, the proliferating cells may be populationally different from those in the adult animals. These possibilities have to be tested in the future by using markers specific to each cell type.

4.2. Neuron-generating lineages

In the present study, no evidence was found that the GFAP-positive cells arose in the HuC/D-positive lineage. Rather, when one of the descendants was HuC/D-positive, most of the other cells in the same lineage were also HuC/D-positive. In some lineages HuC/D-positive cells were generated after several cell divisions. Similarly, when one of the descendants was Prox1- or NeuN-positive, other cells in the same lineage were mostly Prox1- or NeuN-positive. These results suggest the presence of neuron-generating lineages which are destined to produce neurons, although we have no evidence if they are derived from the multipotent type-1 cells or the transiently amplifying type-2, -3 cells.

In the groups of HuC/D-positive lineages, the frequency of cell division was higher in the early DPI period (1–14 DPI) than in the late (15–28 DPI). Almost similar results were observed for the Prox1- or NeuN-positive lineage group. That is, many of the differentiated cells were produced early DPI period in the neuron-generating lineage. We could not find the exact reasons, but it is possible that we are preferentially tracked the cells that are in the later proliferative phase such as the transiently amplifying type-2, -3 cells. This is also the case for our GFAP-positive lineage group. On the other hand, the frequency of cell division was almost even throughout the tracking period in the HuC/D-negative lineage subgroup of unclassified group (Supplementary Fig. S6A). It is possible that the highly proliferative cells were included in this subgroup. The proliferation of HuC/D-negative lineage cells was no less than expected from the prediction (Supplementary Fig. S6B) as the newly divided cells became rarely untraceable.

4.3. Critical traceablility period

While the neuron-generating lineages produced HuC/D-, Prox1- or NeuN-positive descendants, other descendents became frequently untraceable. Once untraceable, these cells never reappeared even under close inspection after immunohistochemistry using anti-EGFP antibody. We also found a significant number of the unclassified lineages in which all the descendents were untraceable before phenotype identification (Supplementary Fig. S5). This is in contrast to the GFAP-positive lineages in which most

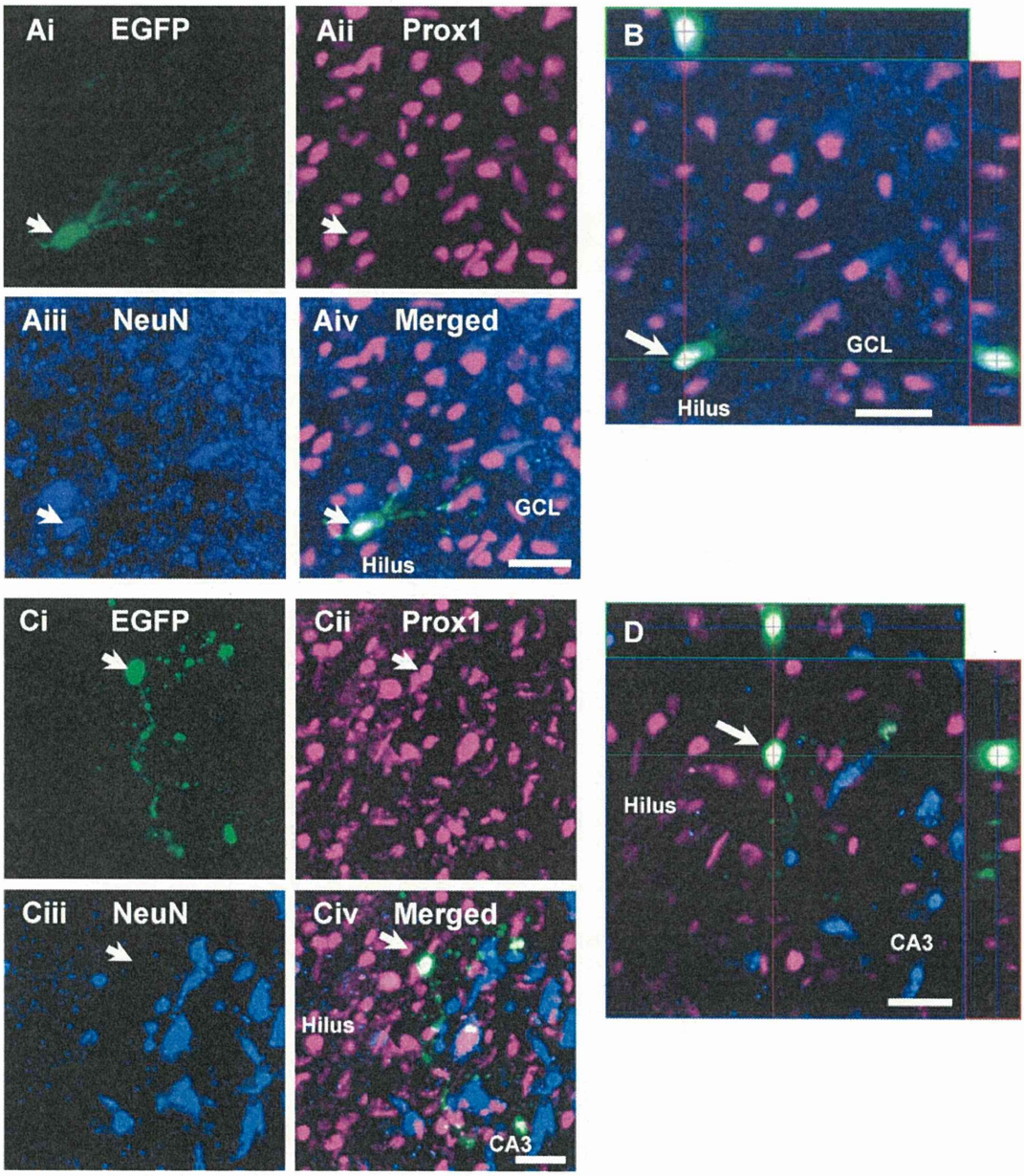

Fig. 6. Immunohistochemical study of differentiation. (A) A mature dentate granule cell layer (GCL) neuron. The phenotype of one of the EGFP-expressing cells (Ai, arrow) was examined immunohistochemically by using either anti-Prox1 antibody (Aii) or anti-NeuN antibody (Aiii). The merged image indicates that this cell is Prox1$^+$/NeuN$^+$ (Aiv) and judged as a mature GCL neuron. (B) Three-dimensional analysis of the cell shown in (Ai–iv). (C) A immature GCL neuron (arrow) that is positive for Prox1 but negative for NeuN, indicated as Prox1$^+$/NeuN$^-$. (D) Three-dimensional analysis of the cell shown in (Ci–iv). Scale bars, 20 μm.

of the descendants were traceable up to 28 DPI. The above postmitotic untraceability is consistent with the previous *in vivo* studies describing that substantial numbers (30–70%) of newly generated cells undergo cell death (Cameron and McKay, 2001; Dayer et al., 2003; Sun et al., 2004). Programmed cell death during normal development has been reported to occur ubiquitously throughout the central and peripheral nervous system of vertebrates and invertebrates (Purves and Lichtman, 1985; Jacobson, 1993; Buss et al., 2006). A quantitative matching of neurons with their targets and afferents is thereby attained. Analogous to the programmed cell death during embryonic period, some of the newly generated neurons might become untraceable as a result of apoptosis (Gould and McEwen, 1993; Krantic et al., 2007) although further study is necessary. It remains possible that some of the cells became untraceable due to other reasons such as migration out of the inspecting fields. However, the incidence of cell untraceability was high during the early postmitotic phase, suggesting the presence of a certain critical period. We refer it as "critical traceability period" to differentiate from the critical period of cell death.

In the postnatal hippocampus, the numbers of newly generated neurons were reduced at a high rate between 6 and 28 days after they were labeled with 5-bromodeoxyuridine (BrdU) but were stable between 1 and 6 months (Dayer et al., 2003; Kempermann et al., 2003). New neurons that expressed GFP by the retrovirus method reduced in density within 3 weeks of virus injection (Tashiro et al., 2006). However, hitherto little has been known about the actual lifespan of newly generated neurons. In the organotypic slice culture of hippocampus the EGFP-labeled new neurons could be tracked as lineages. The critical traceability period was thus measured for individual cells and was 2–14 days after their last division

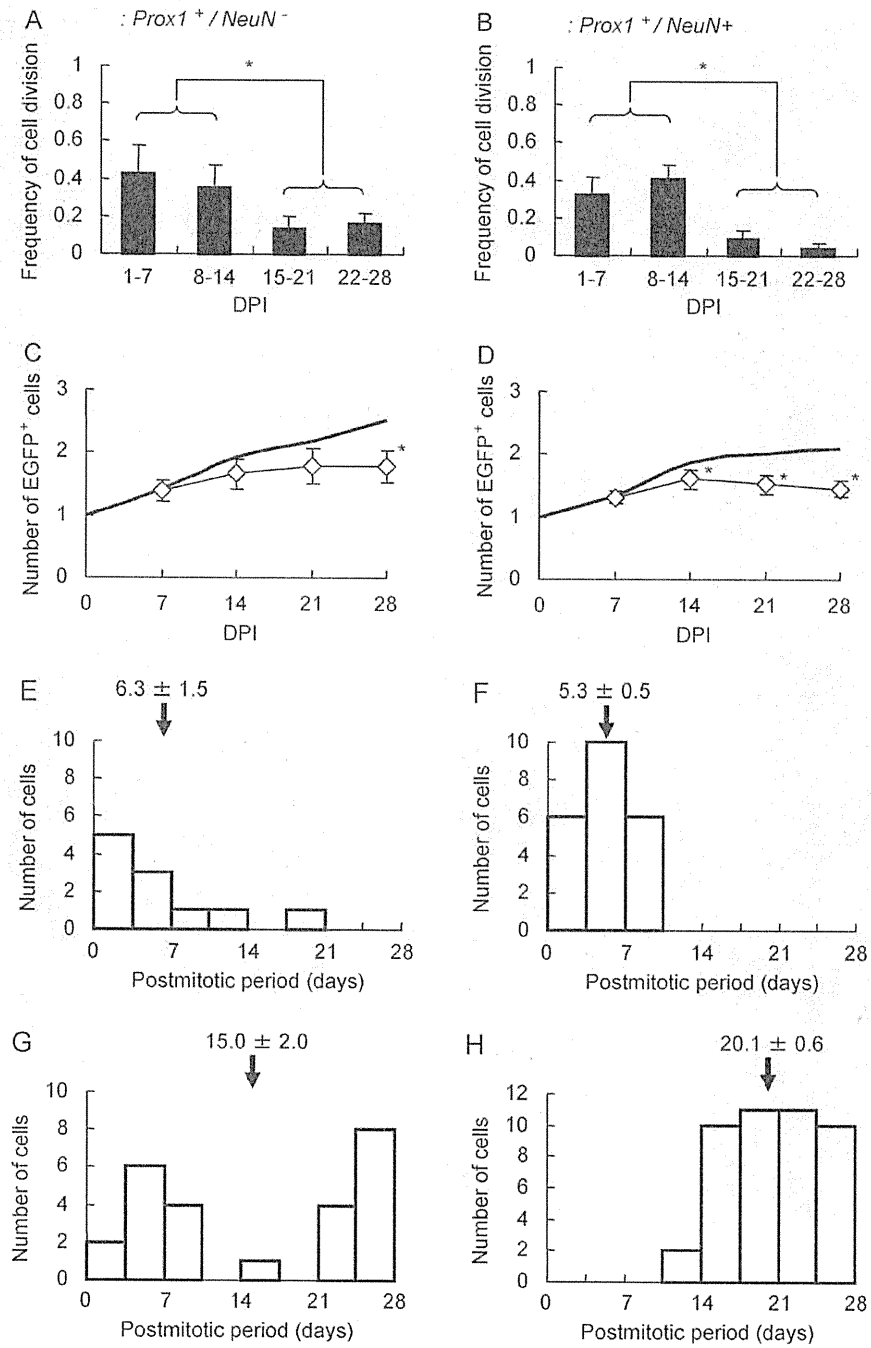

Fig. 7. Analysis of the differentiating lineages. A, C, E and G from the Prox1$^+$/NeuN$^-$ lineages (n = 18) and B, D, F and H from the Prox1$^+$/NeuN$^+$ lineages (n = 34). Note that three lineages were overlapped. (A, B) The frequency of cell division during each of the four period 1–7, 8–14, 15–21 and 22–28 DPI (mean ± SEM). The difference was statistically examined (One-way ANOVA with post hoc Scheffe's F-test) between the early DPI period (1–7 and 7–14) and the later (15–21 and 22–28 DPI). *P < 0.05. (C, D) The time-dependent change of the number of EGFP-expressing cells (open symbols and bars, mean ± SEM). The thick line is the proliferation curve expected from the frequency of cell division (A or B). * indicates the significant difference from the prediction (P < 0.05, One-sample Wilcoxon signed rank test). (E, F) Histograms of the postmitotic periods. Arrows and numbers indicate the mean (±SEM) values. (G, H) Histograms of the postmitotic periods of the immature and mature GCL neurons, respectively. Arrows and numbers indicate the mean (±SEM) values.

in the HuC/D-positive lineages. A similar critical traceability period was observed in both the Prox1$^+$/NeuN$^-$ lineages that generated immature GCL neurons (2–18 days) and the Prox1$^+$/NeuN$^+$ lineages that generated mature GCL neurons (2–10 days). Therefore, it is suggested that a neuron differentiates into its mature form once it survives this period. Consistent with this notion, none of the differentiated GCL neurons that expressed both Prox1 and NeuN had a postmitotic period of less than 12 days. It is possible that a newborn neuron differentiates into its mature form through some key processes that determine its fate.

5. Conclusions

The present experimental system enabled us to track a single progenitor cell and its descendents as a lineage using the organotypic culture of hippocampus as an *ex vivo* model of the post-

natal hippocampus. The lineage was identified retrospectively as neuron-generating using an immunohistochemical marker, HuC/D. We found that (1) the descendent cells of the neuron-generating lineages were mostly GFAP-negative, (2) the newly generated cells became frequently untraceable in the neuron-generating lineages and (3) this critical traceability period was 2–14 days. It is suggested that newly generated neurons differentiate into mature GCL neurons once they survive this period. The adult neurogenesis is under the influence of the local network activity and/or the SGZ niche in the *in vivo* hippocampus (Lie et al., 2005; Ge et al., 2006; Tashiro et al., 2006; Kuwabara et al., 2009). Our lineage analysis methods using slice culture system would be advantageous to test several hypotheses concerning these regulatory mechanisms under experimental manipulations.

Acknowledgements

We thank Y. Sugiyama for technical advice and D.B.L. Teh and B. Bell for language assistance.

Appendix A. Supplementary data

Supplementary data associated with this article can be found, in the online version, at doi:10.1016/j.neures.2010.11.010.

References

Aimone, J.B., Willes, J., Gage, F.H., 2006. Potential role for adult neurogenesis in the encoding of time in new memories. Nat. Neurosci. 9, 723–727.
Akamatsu, W., Fujihara, H., Mitsuhashi, T., Yano, M., Shibata, S., Hayakawa, Y., Okano, J.H., Sakakibara, S., Takano, H., Takano, T., Takahashi, T., Noda, T., Okano, H., 2005. The RNA-binding protein HuD regulates neuronal cell identity and maturation. Proc. Natl. Acad. Sci. U.S.A. 22, 4625–4630.
Alfonoso, L., Guillermo, O., 2007. Prox1 expression patterns in the developing and adult murine brain. Dev. Dyn. 236, 518–524.
Altman, J., Das, G.D., 1965. Autoradiographic and histological evidence of postnatal hippocampal neurogenesis in rats. J. Comp. Neurol. 124, 319–336.
Belachew, S., Chittajallu, R., Aguirre, A.A., Yuan, X., Kirby, M., Anderson, S., Gallo, V., 2003. Postnatal NG2 proteoglycan-expressing progenitor cells are intrinsically multipotent and generate functional neurons. J. Cell Biol. 161, 169–186.
Brown, J.P., Couillard-Després, S., Cooper-Kuhn, C.M., Winkler, J., Aigner, L., Kuhn, H.G., 2003. Transient expression of doublecortin during adult neurogenesis. J. Comp. Neurol. 467, 1–10.
Bruel-Jungerman, E., Laroche, S., Rampon, C., 2005. New neurons in the dentate gyrus are involved in the expression of enhanced long-term memory following environmental enrichment. Eur. J. Neurosci. 21, 513–521.
Bruel-Jungerman, E., Davis, S., Rampon, C., Laroche, S., 2006. Long-term potentiation enhances neurogenesis in the adult dentate gyrus. J. Neurosci. 26, 5888–5893.
Buchs, P.A., Stoppini, L., Muller, D., 1993. Structural modifications associated with synaptic development in area CA1 of rat hippocampal organotypic cultures. Dev. Brain Res. 71, 81–91.
Buss, R.R., Sun, W., Oppenheim, R.W., 2006. Adaptive roles of programmed cell death during nervous system development. Annu. Rev. Neurosci. 29, 1–35.
Cameron, H.A., Woolley, C.S., McEwen, B.S., Gould, E., 1993. Differentiation of newly born neurons and glia in the dentate gyrus of the adult rat. Neuroscience 56, 337–344.
Cameron, H.A., McKay, R.D., 2001. Adult neurogenesis produces a large pool of new granule cells in the dentate gyrus. J. Comp. Neurol. 435, 406–412.
Dailey, M.E., Buchanan, J., Bergles, D.E., Smith, S.J., 1994. Mossy fiber growth and synaptogenesis in rat hippocampal slices in vitro. J. Neurosci. 14, 1060–1078.
Dayer, A.G., Ford, A.A., Cleaver, K.M., Yassaee, M., Cameron, H.A., 2003. Short-term and long-term survival of new neurons in the rat dentate gyrus. J. Comp. Neurol. 460, 563–572.
Dupret, D., Revest, J.M., Koehl, M., Ichas, F., De Giorgi, F., Costet, P., Abrous, D.N., Piazza, P.V., 2008. Spatial relational memory requires hippocampal adult neurogenesis. PLoS ONE 3 (4), e1959, doi:10.1371/journal.pone.0001959.
Eriksson, P.S., Perfilieva, E., Björk-Eriksson, T., Alborn, A.M., Nordborg, C., Peterson, D.A., Gage, F.H., 1998. Neurogenesis in the adult human hippocampus. Nat. Med. 4, 1313–1317.
Ernst, C., Christie, B.R., 2005. The putative neural stem cell marker, nestin, is expressed in heterogeneous cell types in the adult rat neocortex. Neuroscience 138, 183–188.
Filippov, V., Kronenberg, G., Pivneva, T., Reuter, K., Steiner, B., Wang, L.P., Yamaguchi, M., Kettenmann, H., Kempermann, G., 2003. Subpopulation of nestin-expressing progenitor cells in the adult murine hippocampus shows electrophysiological and morphological characteristics of astrocytes. Mol. Cell. Neurosci. 23, 373–382.
Fukuda, S., Kato, F., Tozuka, Y., Yamaguchi, M., Miyamoto, Y., Hisatsune, T., 2003. Two distinct subpopulations of nestin-positive cells in adult mouse dentate gyrus. J. Neurosci. 23, 9357–9366.
Galeeva, A., Treuter, E., Tomarev, S., Pelto-Huikko, M., 2007. A prospero-related homeobox gene Prox-1 is expressed during postnatal brain development as well as in the adult rodent brain. Neuroscience 146, 604–616.
Gähwiler, B.H., 1984. Development of the hippocampus in vitro: cell types, synapses and receptors. Neuroscience 11, 751–760.
Gähwiler, B.H., Capogna, M., Debanne, D., McKinney, R.A., Thompson, S.M., 1997. Organotypic slice cultures: a technique has come of age. Trends Neurosci. 20, 471–477.
Ge, S., Goh, E.L.K., Sailor, K.A., Kitabatake, Y., Ming, G.L., Song, H., 2006. GABA regulates synaptic integration of newly generated neurons in the adult brain. Nature 439, 589–593.
Goldman, S., 2003. Glia as neural progenitor cells. Trends Neurosci. 26, 590–596.
Gould, E., McEwen, B.S., 1993. Neuronal birth and death. Curr. Opin. Neurobiol. 3, 676–682.
Gutierrez, R., Heinemann, U., 1999. Synaptic reorganization in explanted cultures of rat hippocampus. Brain Res. 815, 304–316.
Imayoshi, I., Sakamoto, M., Ohtsuka, T., Takao, K., Miyakawa, T., Yamaguchi, M., Mori, K., Ikeda, T., Itohara, S., Kageyama, R., 2008. Role of continuous neurogenesis in the structural and functional integrity of the adult forebrain. Nat. Neurosci. 11, 1153–1161.
Jacobson, M., 1993. Developmental Neurobiology, third ed. Plenum Press, New York, NY.
Kamada, M., Li, R.Y., Hashimoto, M., Kakuda, M., Okada, H., Koyanagi, Y., Ishizuka, T., Yawo, H., 2004. Intrinsic and spontaneous neurogenesis in the postnatal slice culture of rat hippocampus. Eur. J. Neurosci. 20, 2499–2508.
Kempermann, G., Kuhn, H.G., Gage, F.H., 1997. More hippocampal neurons in adult mice living in an enriched environment. Nature 386, 493–495.
Kempermann, G., Gast, D., Kronenberg, G., Yamaguchi, M., Gage, F.H., 2003. Early determination and long-term persistence of adult-generated new neurons in the hippocampus of mice. Development 130, 391–399.
Kempermann, G., Jessberger, S., Steiner, B., Kronenberg, G., 2004. Milestones of neuronal development in the adult hippocampus. Trends Neurosci. 27, 447–452.
Kempermann, G., 2008. The neurogenic reserve hypothesis: what is adult neurogenesis good for? Trends Neurosci. 31, 163–169.
Krantic, S., Mechawar, N., Reix, S., Quirion, R., 2007. Apoptosis-inducing factor: a matter of neuron life and death. Prog. Neurobiol. 81, 179–196.
Kronenberg, G., Reuter, K., Steiner, B., Brandt, M.D., Jessberger, S., Yamagushi, M., Kempermann, G., 2003. Subpopulations of proliferating cells of the adult hippocampus respond differently to physiologic neurogenic stimuli. J. Comp. Neurol. 467, 455–463.
Kuwabara, T., Hsieh, J., Muotri, A., Yeo, G., Warashina, M., Lie, D.C., Moore, L., Nakashima, K., 2009. Wnt-mediated activation of NeuroD1 and retro-elements during adult neurogenesis. Nat. Neurosci. 12, 1097–1105.
Lagace, D.C., Whitman, M.C., Noonan, M.A., Ables, J.L., DeCarolis, N.A., Arguello, A.A., Donovan, M.H., Fischer, S.J., Farnbauch, L.A., Beech, R.D., DiLeone, R.J., Greer, C.A., Mandyam, C.D., Eisch, A.J., 2007. Dynamic contribution of nestin-expressing stem cells to adult neurogenesis. J. Neurosci. 27, 12623–12629.
Laskowski, A., Schmidt, W., Dinkel, K., Martínez-Sánchez, M., Reymann, K.G., 2005. bFGF and EGF modulate trauma-induced proliferation and neurogenesis in juvenile organotypic hippocampal slice cultures. Brain Res. 1037, 78–89.
Lendahl, U., Zimmerman, L.B., McKay, R.D., 1990. CNS stem cells express a new class of intermediate filament protein. Cell 60, 585–595.
Lie, D.C., Colamarino, S.A., Song, H.J., Désiré, L., Mira, H., Consiglio, A., Lein, E.S., Jessberger, S., Lansford, H., Dearie, A.R., Gage, F.H., 2005. Wnt signalling regulates adult hippocampal neurogenesis. Nature 437, 1370–1375.
Lledo, P.M., Alonso, M., Grubb, M.S., 2006. Adult neurogenesis and functional plasticity in neuronal circuits. Nat. Rev. Neurosci. 7, 179–193.
Meshi, D., Drew, M.R., Saxe, M., Ansorge, M.S., David, D., Santarelli, L., Malapani, C., Moore, H., Hen, R., 2006. Hippocampal neurogenesis is not required for behavioral effects of environmental enrichment. Nat. Neurosci. 9, 729–731.
Namba, T., Mochizuki, H., Onodera, M., Mizuno, Y., Namiki, H., Seki, T., 2005. The fate of neural progenitor cells expressing astrocytic and radial glial markers in the postnatal rat dentate gyrus. Eur. J. Neurosci. 22, 1928–1941.
Namba, T., Mochizuki, H., Onodera, M., Namiki, H., Seki, T., 2007. Postnatal neurogenesis in hippocampal slice cultures: early in vitro labeling of neural precursor cells leads to efficient neuronal production. J. Neurosci. Res. 85, 1704–1712.
Okada, M., Sakaguchi, T., Kawasaki, K., 1995. Correlation between anti-ubiquitin immunoreactivity and region-specific neuronal death in N-methyl-D-aspartate-treated rat hippocampal organotypic cultures. Neurosci. Res. 22, 359–366.
Palmer, T.D., Takahashi, J., Gage, F.H., 1997. The adult rat hippocampus contains primordial neural stem cells. Mol. Cell. Neurosci. 8, 389–404.
Poulsen, F.R., Blaabjerg, M., Montero, M., Zimmer, J., 2005. Glutamate receptor antagonists and growth factors modulate dentate granule cell neurogenesis in organotypic, rat hippocampal slice cultures. Brain Res. 1051, 35–49.
Purves, D., Lichtman, J.W., 1985. Principles of Neural Development. Sinauer Associates, Inc., Sunderland, MA.
Raineteau, O., Rietschin, L., Gradwohl, G., Guillemot, F., Gähwiler, B.H., 2004. Neurogenesis in hippocampal slice cultures. Mol. Cell. Neurosci. 26, 241–250.
Rivers, L.E., Young, K.M., Rizzi, M., Jamen, F., Psachoulia, K., Wada, A., Kessaris, N., Richardson, W.D., 2008. PDGFRA/NG2 glia generate myelinating oligodendrocytes and piriform projection neurons in adult mice. Nat. Neurosci. 11, 1392–1401.

Robain, O., Barbin, G., Billette de Villemeur, T., Jardin, L., Jahchan, T., Ben-Ari, Y., 1994. Development of mossy fiber synapses in hippocampal slice culture. Dev. Brain Res. 80, 244–250.
Roybon, L., Hjalt, T., Stott, S., Guillemot, F., Li, J.Y., Brundin, P., 2009. Neurogenin2 directs granule neuroblast production and amplification while NeuroD1 specifies neuronal fate during hippocampal neurogenesis. PLoS ONE 4 (3), e4779, doi:10.1371/journal.pone.0004779.
Sakaguchi, T., Okada, M., Kawasaki, K., 1994. Sprouting of CA3 pyramidal neurons to the dentate gyrus in rat hippocampal organotypic cultures. Neurosci. Res. 20, 157–164.
Saxe, M.D., Battaglia, F., Wang, J.W., Malleret, G., David, D.J., Monckton, J.E., Garcia, A.D., Sofroniew, M.V., Kandel, E.R., Santarelli, L., Hen, R., Drew, M.R., 2006. Ablation of hippocampal neurogenesis impairs contextual fear conditioning and synaptic plasticity in the dentate gyrus. Proc. Natl. Acad. Sci. U.S.A. 103, 17501–17506.
Seki, T., Namba, T., Mochizuki, H., Onodera, M., 2007. Clustering, migration, and neurite formation of neural precursor cells in the adult rat hippocampus. J. Comp. Neurol. 502, 275–290.
Seri, B., García-Verdugo, J.M., McEwen, B.S., Alvarez-Buylla, A., 2001. Astrocytes give rise to new neurons in the adult mammalian hippocampus. J. Neurosci. 21, 7153–7160.
Seri, B., García-Verdugo, J.M., Collado-Morente, L., McEwen, B.S., Alvarez-Buylla, A., 2004. Cell types, lineage, and architecture of the germinal zone in the adult dentate gyrus. J. Comp. Neurol. 478, 359–378.
Steiner, B., Kronenberg, G., Jessberger, S., Brandt, M.D., Reuter, K., Kempermann, G., 2004. Differential regulation of gliogenesis in the context of adult hippocampal neurogenesis in mice. Glia 46, 41–52.
Steiner, B., Klempin, F., Wang, L.P., Kott, M., Kettenmann, H., Kempermann, G., 2006. Type-2 cells as link between glial and neuronal lineage in adult hippocampal neurogenesis. Glia 54, 805–814.
Steiner, B., Zurborg, S., Hrster, H., Fabel, K., Kempermann, G., 2008. Differential 24 h responsiveness of prox1-expressing precursor cells in adult hippocampal neurogenesis to physical activity, environmental enrichment, and kainic acid-induced seizures. Neuroscience 154, 521–529.
Stoppini, L., Buchs, P.A., Muller, D., 1991. A simple method for organotypic cultures of nervous tissue. J. Neurosci. Methods 37, 173–182.
Sun, W., Winseck, A., Vinsant, S., Park, O.H., Kim, H., Oppenheim, R.W., 2004. Programmed cell death of adult-generated hippocampal neurons is mediated by the proapoptotic gene Bax. J. Neurosci. 24, 11205–11213.
Tashiro, A., Sandler, V.M., Toni, N., Zhao, C., Gage, F.H., 2006. NMDA-receptor-mediated, cell-specific integration of new neurons in adult dentate gyrus. Nature 442, 929–933.
Thallmair, M., Ray, J., Stallcup, W.B., Gage, F.H., 2006. Functional and morphological effects of NG2 proteoglycan deletion on hippocampal neurogenesis. Exp. Neuro. 202, 167–178.
van Praag, H., Christie, B.R., Sejnowski, T.J., Gage, F.H., 1999. Running enhances neurogenesis, learning, and long-term potentiation in mice. Proc. Natl. Acad. Sci. U.S.A. 96, 13427-13431.72.
Wakamatsu, Y., Weston, J.A., 1997. Sequential expression and role of Hu RNA-binding proteins during neurogenesis. Development 124, 3449–3460.
Zhang, C.L., Zou, Y., He, W., Gage, F.H., Evans, R., 2008. A role for adult TLX-positive neural stem cells in learning and behaviour. Nature 451, 1004–1007.
Zhu, X., Bergles, D.E., Nishiyama, A., 2008. NG2 cells generate both oligodendrocytes and gray matter astrocytes. Development 135, 145–157.
Zimmer, J., Gähwiler, B.H., 1984. Cellular and connective organization of slice cultures of the rat hippocampus and fascia dentata. J. Comp. Neurol. 228, 432–446.

Glossary

BrdU: 5-bromodeoxyuridine
GCL: granule cell layer
EGFP: enhanced green fluorescent protein
GFAP: glial fibrillary acidic protein
NeuN: neuronal nuclei antigen
PBS: phosphate-buffered saline
Prox1: prospero-related homeobox protein
PSA-NCAM: polysialyated neural cell adhesion molecule
SGZ: subgranular zone

Neuroscience Research 71 (2011) 328–334

Contents lists available at SciVerse ScienceDirect

Neuroscience Research

journal homepage: www.elsevier.com/locate/neures

Evaluation of a Sindbis virus vector displaying an immunoglobulin-binding domain: Antibody-dependent infection of neurons in living mice

Ayumu Konno[a,b,c,*], Tatsuya Honjo[a,b], Atsushi Uchida[a], Toru Ishizuka[a,b], Hiromu Yawo[a,b,c,d]

[a] Department of Developmental Biology and Neuroscience, Tohoku University Graduate School of Life Sciences, Sendai 980-8577, Japan
[b] JST, CREST, Tokyo 102-0075, Japan
[c] Tohoku University Basic and Translational Research Centre for Global Brain Science, Sendai 980-8575, Japan
[d] Center for Neuroscience, Tohoku University Graduate School of Medicine, Sendai 980-8575, Japan

ARTICLE INFO

Article history:
Received 11 June 2011
Received in revised form 29 August 2011
Accepted 31 August 2011
Available online 8 September 2011

Keywords:
Sindbis virus
Gene delivery
Stereotaxic injection
Antigen–antibody reaction

ABSTRACT

Viral vectors that genetically incorporate an immunoglobulin-binding domain on their surfaces provide many advantages because of the availability of a spectrum of antibodies that allow the selection of a wide range of target cells. However, the specificity and the effectiveness of this system have not been evaluated in the field of neuroscience. We investigated the effectiveness and specificity of a recombinant Sindbis virus displaying an antibody-binding domain of bacterial protein A (ZZ Sindbis). We found that the ZZ Sindbis virus vector specifically infected hippocampal neurons in an antibody-specific manner in living mice, although the efficiency of the gene transduction was not high. However, the ZZ Sindbis virus vector that did not display any specific antibodies continued to exhibit intrinsic tropism toward Bergmann glial cells in the cerebellum. These data indicate that the antibody-displaying viral vectors are potentially useful for delivering a gene of interest to a specific subset of neurons in the central nervous system with the help of neuron type-specific antibodies.

1. Introduction

Viral vectors have been powerful research tools for both *in vivo* and *in vitro* studies because of their ease of use and efficient transfection. The cell-targeted expression of a gene is typically accomplished using cell type-specific promoters (Portales-Casamar et al., 2010). This strategy, however, has several disadvantages such as virus toxicity; the promoter is only capable of regulating the expression of the transgene and does not suppress the infection by the viral vector. The expression of the transgene in the target cells may be insufficient because of weak induction by the specific promoter. Moreover, the length of specific promoter regions is sometimes too large to package a viral vector.

Recently, a variety of molecular engineering approaches for modifying the tropism of a virus for a particular cell type have been reported for clinical use in cell-targeting gene therapy (Schaffer et al., 2008; Waehler et al., 2007). Viral vectors that genetically incorporate an immunoglobulin (Ig)-binding domain on their surfaces (Korokhov et al., 2003; Ohno et al., 1997; Ried et al., 2002; Tai et al., 2003) provide a number of advantages because of the availability of a spectrum of antibodies that allow the selection of a wide range of target cells. These viral vectors can selectively infect a specific subset of cells and facilitate the expression of exogenous genes under a variety of regulation strategies (e.g., active promoter or induction mediated by other factors). However, the specificity and the effectiveness of this system have not been evaluated in the field of neuroscience.

In the present study, we investigated the effectiveness and specificity of a recombinant Sindbis virus that displayed an IgG-binding domain of bacterial protein A (Ohno et al., 1997). We showed that this recombinant Sindbis virus vector specifically infected a subtype of hippocampal neurons in an antibody-specific manner in living mice, although the efficiency of the gene transduction was not high. Our results suggest that viral vectors incorporating an IgG-binding domain can be used to deliver a gene of interest to a specific subset of neurons in the central nervous system (CNS) with the help of neuron type-specific antibodies. However, this viral vector that did not display any specific antibodies continued to exhibit intrinsic tropism toward some cells, such as Bergmann glial cells in the cerebellum.

2. Materials and methods

2.1. Cell culture

Baby hamster kidney (BHK) cells were grown in OptiPRO SFM medium (Invitrogen Life Technologies, Carlsbad, CA) supplemented with 200 mM L-glutamine (Sigma–Aldrich, St. Louis, MO). PC12 cells

* Corresponding author. Present address: Department of Neurophysiology, Gunma University Graduate School of Medicine, Maebashi, Gunma 371-8511, Japan. Tel.: +81 27 220 7934; fax: +81 27 220 7936.
E-mail address: konnoa@gunma-u.ac.jp (A. Konno).

0168-0102/$ – see front matter © 2011 Elsevier Ireland Ltd and the Japan Neuroscience Society. All rights reserved.
doi:10.1016/j.neures.2011.08.013

were cultured in RPMI-1640 medium (Invitrogen Life Technologies) supplemented with 10% fetal bovine serum (FBS; Biological Industries, Beit Haemek, Israel) and antibiotics (penicillin and streptomycin; Invitrogen Life Technologies).

2.2. Animals

All animal experiments were approved by the Institutional Animal Care and Use Committee of the Tohoku University Environmental & Safety Committee and were conducted in accordance with the Guidelines for Animal Experiments and Related Activities in Tohoku University and with the guiding principles of the Physiological Society of Japan and the NIH.

2.3. Plasmid construction

The plasmid ZZ SINDBIS m168 (Morizono and Chen, 2005; Morizono et al., 2005) was kindly provided by Dr. Irvin S.Y. Chen (UCLA AIDS Institute, Los Angeles, CA). ZZ SINDBIS m168 was the envelope plasmid for the production of the pseudotyped lentiviral vector and contained a ZZ domain derived from the IgG-binding domain of protein A (Nilsson et al., 1987) that was inserted into the modified E2 domain of the Sindbis virus. This modified envelope gene was transferred into a DH-BB helper plasmid (Bredenbeek et al., 1993) to produce a recombinant Sindbis virus. Briefly, the modified E2 envelope gene containing a ZZ domain and the inverse fragment of the DH-BB gene were amplified by polymerase chain reaction (PCR) using ZZ SINDBIS m168 and DH-BB as templates, respectively. The oligonucleotides 5′-GCACCACTAGTCACGGCAATGTGTTTGC-3′ and 5′-TCACGGCGCGCTTTACAGGCACATAACACT-3′ were used as primers for the modified E2 domain, and 5′-GTAAAGCGCGCCGTGAGTGCCTGACGCC-3′ and 5′-ATTGCCGTGACTAGTGGTGCTGCGGA-3′ were used as primers for the inverse fragment. Each primer contained a unique restriction enzyme BssHII or SpeI site. The resulting PCR products were digested with BssHII and SpeI and were ligated to each other. They were then transformed into Competent High-DH5α (Toyobo Co., Osaka, Japan). The nucleotide sequence of the modified E2 domain was confirmed by DNA sequencing, and the DH-BB-ZZ m168 was obtained.

2.4. Recombinant Sindbis pseudovirion production

Expression vectors harboring the fluorescent protein Venus (Nagai et al., 2002) or mCherry (Shaner et al., 2004), which were named pSinRep5-Venus or pSinRep5-mCherry (Ishizuka et al., 2006), respectively, were used for production of the recombinant Sindbis pseudovirions. RNAs were transcribed from pSinRep5-Venus or pSinRep5-mCherry and DH-BB-ZZ m168 DNA using MEGAscript SP6 Kit (Ambion, Austin, TX). BHK cells were electroporated with these RNAs and were grown for 10 h at 37 °C under 5% CO_2 in MEM alpha medium (Invitrogen Life Technologies) that contained 5% FBS. The cells were then incubated in OptiPRO SFM medium supplemented with 200 mM L-glutamine without FBS. After 24 h, the culture supernatant was harvested, and aliquots were stored at −80 °C. Likewise, the control recombinant Sindbis pseudovirions were generated using the plasmids pSinRep5-Venus and DH-BB. In this way, we produced three types of Sindbis pseudovirions, which were designated ZZ Sindbis-Venus, ZZ Sindbis-mCherry, and DH-BB-Venus.

2.5. In vitro infection assay

To quantify the infection titers of ZZ Sindbis-Venus in the presence or absence of the antibody, rat pheochromocytoma PC12 cells were used as the target cells. The viral solution was mixed with or without the antibody against the extracellular domain of $p75^{NTR}$ (ANT-007; Alomone Labs, Jerusalem, Israel), which is one of the low affinity nerve growth factor receptors and is specifically expressed on the membrane of PC12 cells. After 1 h of incubation at 37 °C, 400 μl of the 10-fold serial dilution of the mixture was added to 50% confluent PC12 cells on 6-well plates. After 1 h of incubation at 37 °C under 5% CO_2, 2 ml of RPMI-1640 with 1% FBS was added to each well. At 24 h postinfection, the number of cells expressing the fluorescence protein was counted using a conventional fluorescent microscopy (Axiovert 200, Carl Zeiss, Göttingen, Germany).

2.6. In vivo infection assay

We used the transgenic mouse TV-42, which specifically expressed synaptopHluorin in a restricted region of the hippocampus (Araki et al., 2005), for targeting. Two microliters of the viral solution containing ZZ Sindbis-mCherry with the GFP antibody (a generous gift from Drs. T. Kaneko and K. Nakamura, Kyoto University, Japan) was stereotaxically injected into the dentate hilus of the TV-42 mice. As a negative control, ZZ Sindbis with GFP antibody was injected into wild-type C57BL/6J mice. The injections of ZZ Sindbis-Venus into the cerebellum were performed on the wild-type mice. For all the injection experiments, the mice (4–6 weeks old, 13–17 g BW) were anesthetized via an intraperitoneal injection of a ketamine–xylazine mixture (50 mg/kg BW ketamine, Daiichi Sankyo Co. Ltd., Tokyo, Japan, and 10 mg/kg BW xylazine, Sigma–Aldrich, St. Louis, MO, USA). Two days after the injection, the mice were ether-anesthetized and decapitated, and the whole brains were quickly removed. The removed brain was rapidly immersed in ice-cold ethanol for 60 min and then in ice-cold methanol for 40 min. The dehydrated brain was embedded in 2.5% agarose gel, and coronal brain slices 250–300 μm in thickness were prepared using a vibratome (Leica, VT1000s, Wetzlar, Germany). The brain slices were observed under an inverted fluorescent microscope (Axiovert 200, Carl Zeiss).

2.7. Immunohistochemistry

The coronal brain slices were fixed at room temperature with 4% paraformaldehyde (PFA) in PBS (0.1 M, pH 7.4) for 30 min, blocked with 100% BlockingOne (Nacalai Tesque, Kyoto, Japan), and treated overnight at 4 °C in PBS containing 5% BlockingOne and 0.1% Triton X-100 with three antibodies: rat monoclonal anti-GFP (1:2000; Nacalai Tesque; cross-reactive to pHluorin), rabbit polyclonal anti-DsRed (1:2000; Clontech, Palo Alto, CA, USA; cross-reactive to mCherry) and mouse monoclonal anti-NeuN (1:2000; Chemicon, Temecula, CA, USA; marker for mature neuron). After washing four times at room temperature in PBS with 0.1% Triton X-100, the slices were treated with secondary antibodies in PBS containing 5% BlockingOne and 0.1% Triton X-100 for 3 h. Alexa Fluor 488-conjugated goat anti-rat IgG (1:200; Invitrogen), Alexa Fluor 546-conjugated goat anti-rabbit IgG (1:200; Invitrogen), and Alexa Fluor 633-conjugated goat anti-mouse IgG (1:200; Invitrogen) were used as secondary antibodies. Finally, the slices were washed four times in PBS with 0.1% Triton X-100 at room temperature and were mounted on glass slides with Permafluor (Thermo Fisher Scientific, Waltham, MA). Each specimen was examined under a confocal laser scanning microscopy (LSM510META, Carl Zeiss).

3. Results

3.1. In vitro infection assay

The p75 neurotrophin receptor ($p75^{NTR}$) is a member of the tumor necrosis factor receptor superfamily and plays many roles in

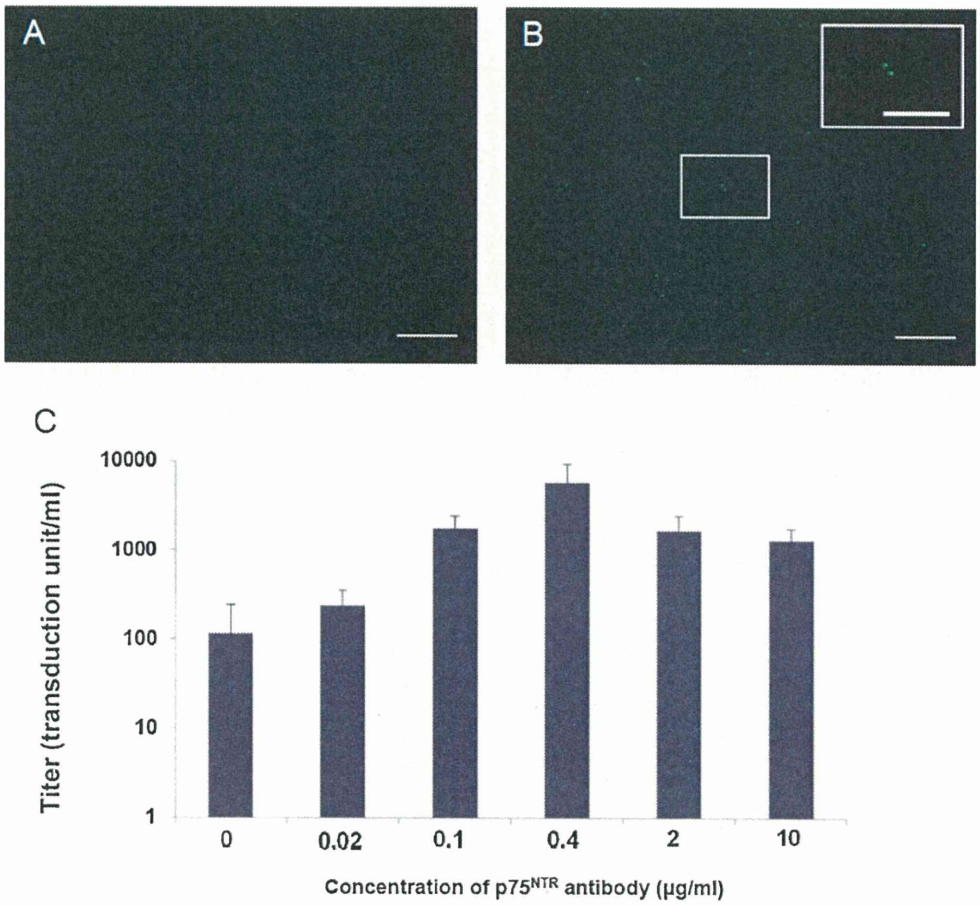

Fig. 1. ZZ Sindbis-Venus with $p75^{NTR}$ antibody infected PC12 cells. (A) PC12 cells treated with ZZ Sindbis without the antibody (bar: 500 μm). (B) PC12 cells treated with ZZ Sindbis with 0.4 μg/ml of the antibody (bar: 500 μm). The inset shows a magnified image of a Venus-expressing cell (bar: 250 μm). (C) Antibody-dependent infectivity titers of ZZ Sindbis-Venus, which is a viral vector displaying immunoglobulin-binding domains. To investigate the dependency of ZZ Sindbis on the concentration of the antibody, PC12 cells were treated with ZZ Sindbis-Venus mixed with various concentrations of $p75^{NTR}$ antibody (p75 Ab), which is shown as the weight of the antibody (μg) per virus solution volume (ml). Titers were calculated by counting the number of cells that expressed Venus. The values shown were obtained from three independent experiments, and the error bars represent standard deviations.

the differentiation, apoptosis, modulation of axonal elongation and synaptic plasticity in the nervous system (Chao, 2003; Dechant and Barde, 2002; Kaplan and Miller, 2000). As each PC12 cell expresses $p75^{NTR}$ molecules in its plasma membrane (Niederhauser et al., 2000), it can be expected that the cells may be transfected with viral genes via ZZ Sindbis pseudovirion vectors in the presence, but not in the absence, of anti-$p75^{NTR}$ antibodies that target the extracellular domain. This was examined using ZZ Sindbis pseudovirions encoding Venus, which is one of the GFP derivatives. As shown in Fig. 1A, the expression of this marker was negligible in the absence of anti-$p75^{NTR}$ antibodies. However, two to three hundred PC12 cells treated with a tenfold diluted virus solution expressed the marker in the presence of the antibody at a concentration of 0.4 μg/ml (Fig. 1B). We then calculated the infectivity titers of the recombinant Sindbis pseudovirions for various concentrations of $p75^{NTR}$ antibodies, taking the number of cells that expressed fluorescent protein Venus as a marker (Fig. 1C). Although the highest percentage of transduced cells was less than 1% and gene transduction was very inefficient, the infectivity titer of ZZ Sindbis-Venus was dependent on the concentration of the antibody, with a positive relationship at lower antibody concentrations and a negative relationship at higher concentrations. This result was likely due to an excess of antibodies binding to the $p75^{NTR}$ and thus competitively inhibiting the antibody-displaying ZZ Sindbis pseudovirions from targeting the molecule.

3.2. *In vivo infection assay in hippocampus*

Synaptobrevin/VAMP-2 is one of the vesicular membrane proteins of small synaptic vesicles in the presynaptic terminal and is involved in docking/priming during exocytosis as one of the SNARE complex elements (Horikawa et al., 1993; Söllner et al., 1993). When this protein is fused with a pH-sensitive derivative of green fluorescent protein (pHluorin) at its intra-lumenal C-terminal, the fusion protein (syanptopHluorin, SpH) increases its fluorescence with vesicular exocytosis and decreases fluorescence with endocytosis and the subsequent reacidification of the intravesicular space (Miesenböck et al., 1998; Yuste et al., 2000; Sankaranarayanan et al., 2000). We recently described the mouse line TV-42, which selectively expressed SpH in the presynaptic boutons of dentate granule cells and the CA1 pyramidal cells of the hippocampus (Araki et al., 2005). As some of the SpH molecules are also distributed in the plasma membrane (Sankaranarayanan et al., 2000; Araki et al., 2005), they can be expected to react with anti-GFP IgGs in the extracellular space.

When the ZZ Sindbis-mCherry was injected into the hippocampus of TV-42 mice with anti-GFP IgGs, red fluorescence was observed in the granule cells of the dentate gyrus (Fig. 2A) and in the pyramidal cells of the hippocampal CA1 region (Fig. 2B). The number of mCherry-expressing neurons varied from trial to trial in our *in vivo* transduction, which was likely due to uncontrollable

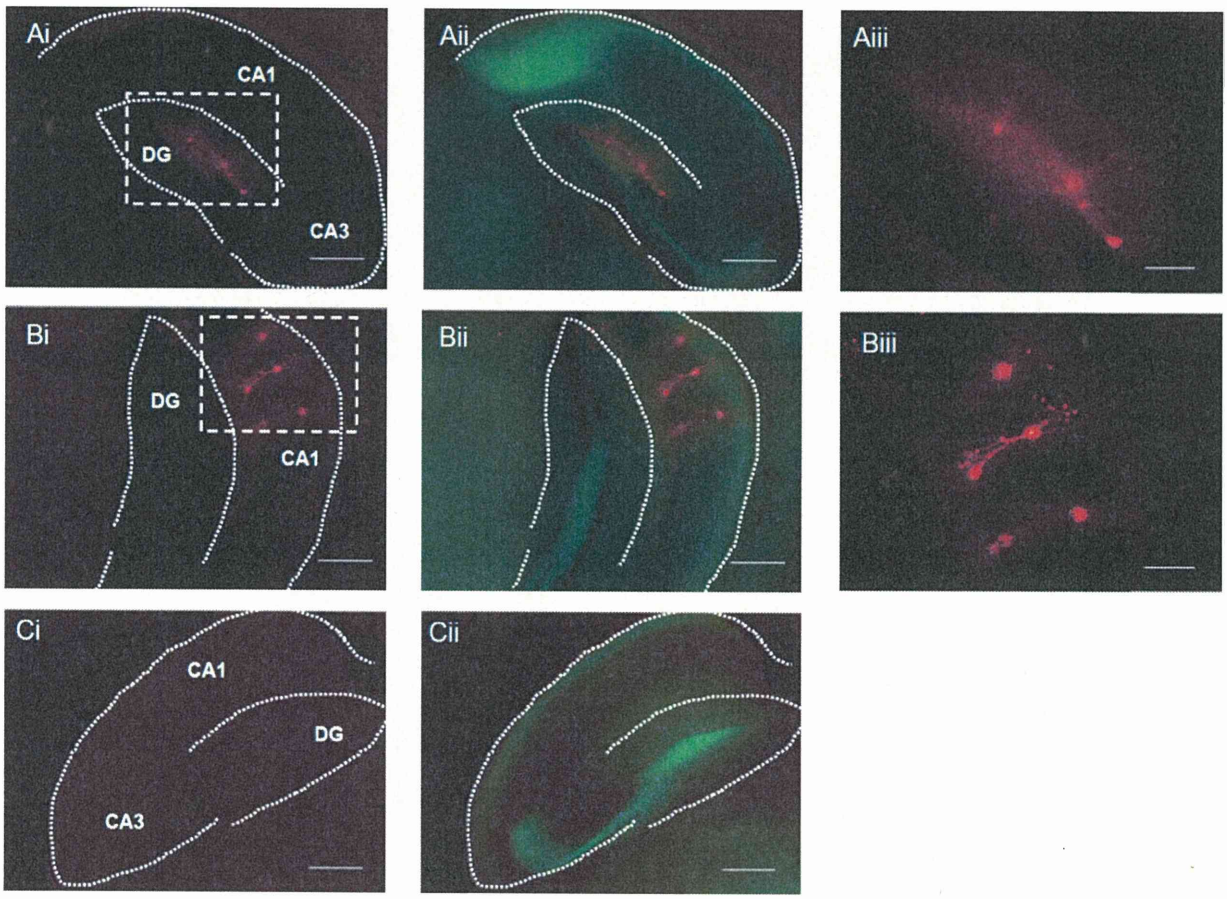

Fig. 2. Fluorescent microscopic images of sliced TV-42 hippocampus that was injected with ZZ Sindbis encoding mCherry. Green or red fluorescence shows either the expression of pHluorin or mCherry, respectively. (Ai–iii) ZZ Sindbis-mCherry with GFP antibody infected in the dentate gyrus. (Bi–iii) ZZ Sindbis-mCherry with GFP antibody infected in the CA1 region. (Ci and ii) ZZ Sindbis-mCherry without antibody. Magnified images of the areas enclosed by the dotted lines in Ai and Bi are indicated in Aiii and Biii, respectively. DG, dentate gyrus. Scale bars: 500 μm (Ai and ii, Bi and ii, Ci and ii); 100 μm (Aiii and Biii).

factors such as the precise site of injection and the diffusion of the viral solution, but it ranged from 2 to 20 neurons in the hippocampus of 6 trials. ZZ Sindbis-mCherry apparently targeted these cells through the binding of the anti-GFP antibody that was displayed on the surface of the viral vector to pHluorin that was expressed in the extracellular surface of the plasma membrane. In contrast, without the antibody, no cells in the hippocampus of the TV-42 mice expressed mCherry (Fig. 2C). Similarly, the mCherry-fluorescence was not detectable in any hippocampal cells of the wild-type C57BL/6J mice, even two days after the injection of ZZ Sindbis-mCherry with the anti-GFP antibody (data not shown).

The ZZ Sindbis-mediated expression of mCherry was also examined in detail using DsRed immunohistochemistry (Fig. 3A). The mCherry-expressing cell shown in Fig. 3A was judged as a CA1 pyramidal neuron of the hippocampus by its position and shape (magnified image in Supplementary Fig. S1). We also detected granule cells of the dentate gyrus using the same immunohistochemical method (Fig. 3B). However, no other types of cells, such as dentate hilar neurons, CA3 neurons or GABAergic interneurons, were identified as positive for mCherry even after immunohistochemistry. The expression of mCherry was also negligible in cells from non-neuronal populations.

3.3. *In vivo infection assay in the cerebellum*

The specificity of the ZZ Sindbis pseudovirion was also tested in the cerebellum. However, the pseudovirion was found to exhibit some tropism toward Bergmann glial cells even in the absence of all antibodies (Fig. 4A). The control DH-BB Sindbis virus also showed strong tropism toward Bergmann glial cells (Fig. 4B). Even at low titers of viral vectors, a number of Bergmann glial cells expressed Venus fluorescence with negligible expression in the neuronal population.

4. Discussion

In the present study, we used ZZ Sindbis, a viral vector engineered to display an IgG-binding domain of protein A, to evaluate the specificity and effectiveness of antibody-displaying viral vectors in the CNS. As these vectors are capable of binding to the target cells by utilizing only antibodies for their cell-surface molecules, it was considered possible for the vectors to deliver an intended gene to a certain subset of neurons in an antibody-specific manner (Fig. 5). Consistent with this expectation, ZZ Sindbis was found capable of cell-specific infection in two combination systems of antibody and target: anti-$p75^{NTR}$ antibody and PC12 cells, which is a well-established model for sympathetic neurons (Fig. 1), and an anti-GFP antibody and TV-42 transgenic mice (Figs. 2 and 3). In particular, the infected neurons in the hippocampus of TV-42 mice were limited to pyramidal neurons in the CA1 and granule cells in the dentate gyrus. Because pHluorin molecules are exclusively expressed in these hippocampal neurons of TV-42 mice (Fig. 3; Araki et al., 2005), the above observation is consistent with the

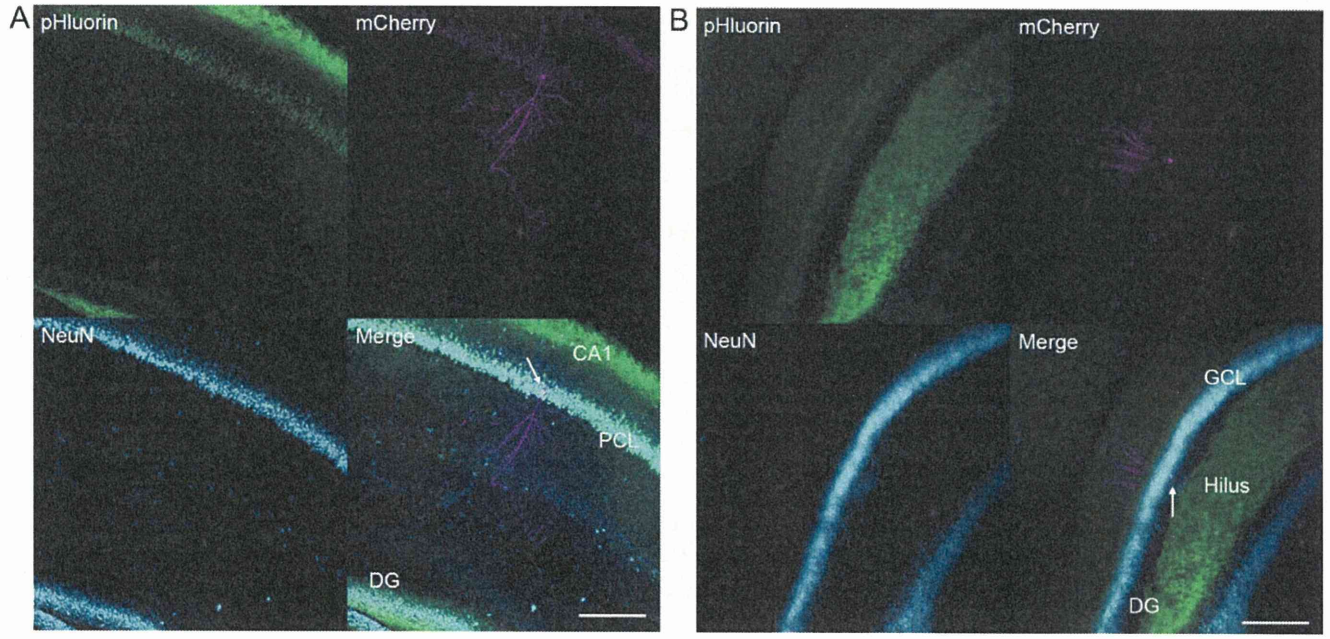

Fig. 3. Antibody-dependent infection of ZZ Sindbis in the hippocampus of a TV-42 transgenic mouse. A neuron expressing mCherry was identified immunohistochemically by anti-GFP (pHluorin), anti-DsRed (mCherry) and anti-NeuN (NeuN), a marker of the neuronal soma. (A) CA1 region. Note that some CA1 pyramidal cells and their presynaptic boutons were reactive to anti-GFP because of the expression of synaptopHluorin. The arrow indicates a typical CA1 pyramidal cell. (B) Dentate gyrus. Some presynaptic boutons in the hilus are reactive to anti-GFP because of the expression of synaptopHluorin. The arrow indicates a typical granule cell. DG, dentate gyrus; PCL, pyramidal cell layer; GCL, granule cell layer. Bar: 200 μm.

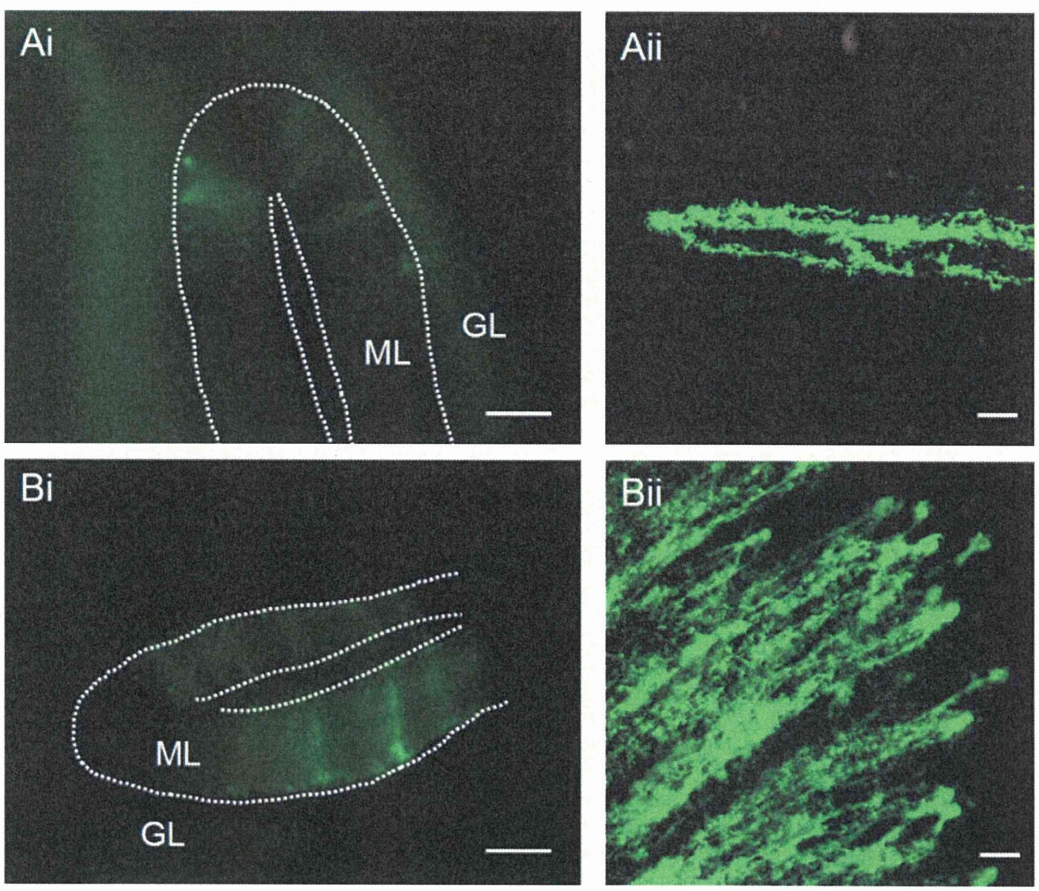

Fig. 4. Background infection. (Ai and ii) Cerebellar cells infected by ZZ Sindbis-Venus without antibody. Note that these cells were judged as Bergmann glial cells on the basis of their positions and shapes. (Bi and ii) Cerebellar cells infected by the control DH-BB-Venus. Ai and Bi are the microscopic images of Venus fluorescence (scale bars, 100 μm). Aii and Bii are images enhanced with anti-GFP immunohistochemistry (scale bars, 20 μm). ML, molecular layer; GL, granular layer.

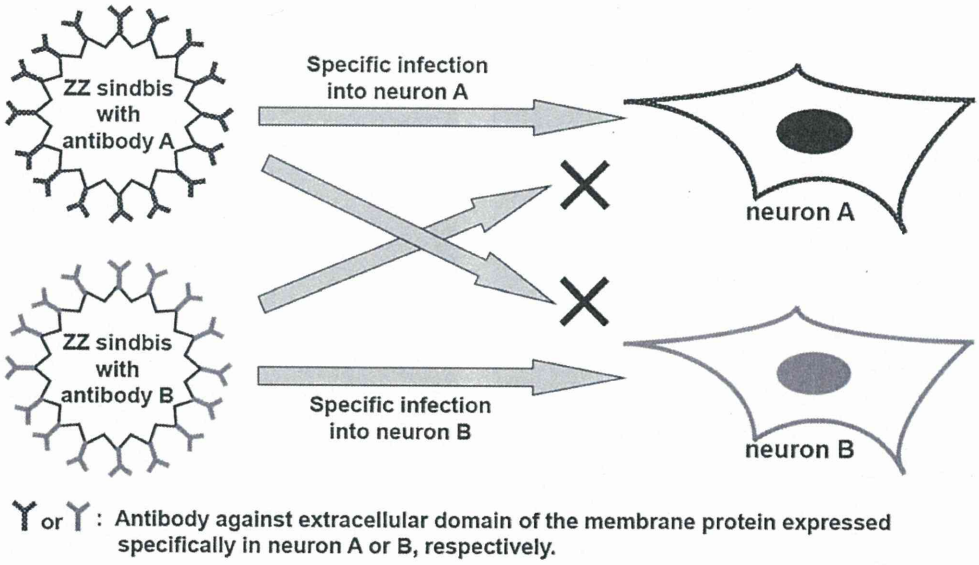

Fig. 5. Targeted infection of a neuron with the combination of ZZ Sindbis and cell-type specific antibodies (hypothesis).

idea that ZZ Sindbis-mCherry infects cells through the binding of an anti-GFP antibody to pHluorin.

ZZ Sindbis was generated by a recombination of the Sindbis virus, an enveloped virus with a single-stranded RNA genome (Ohno et al., 1997). The Sindbis virus vector has advantages in terms of its high expression levels and its rapid induction of foreign genes (Bredenbeek et al., 1993; Huang, 1996). Indeed, the gene expression induced by ZZ Sindbis could be observed within 12 h both *in vitro* and *in vivo*. Sindbis virus is also known to exhibit severe toxicity (Frolov and Schlesinger, 1994; Nargi-Aizenman and Griffin, 2001). However, the membrane properties, such as resting potential, input resistance and membrane time constant, of Sindbis-infected cells were the same as those of non-infected cells 12–24 h after inoculation (Ishizuka et al., 2006). Furthermore, Maletic-Savatic and colleagues reported that neurons infected with the Sindbis virus were physiologically healthy until at least day 3 postinfection (Maletic-Savatic et al., 1999). In our experiments, the 48-h post-transfection neurons with ZZ Sindbis showed no abnormality in their appearances (Figs. 2–4).

The Sindbis virus contains two envelope glycoproteins: E1, which mediates the fusion of the viral envelope with the target cell membrane, and E2, which mediates its binding to target cells (Garoff et al., 1994). As the ZZ domain was inserted into the E2 region, ZZ Sindbis showed reduced background infection levels (Ohno et al., 1997). Morizono and colleagues performed alanine substitutions for a number of amino acids that were reported to affect binding (Morizono et al., 2005). These mutations of E2 in ZZ Sindbis appreciably reduced the nonspecific infections. We used this modified envelope glycoprotein and found that ZZ Sindbis lacking antibodies rarely infected PC12 cells and hippocampus neurons (Figs. 1 and 2C). Unexpectedly, ZZ Sindbis was found to infect Bergmann glial cells in the cerebellum in an antibody-independent manner (Fig. 4A). This phenomenon may be attributable to the intrinsically robust tropism of the control Sindbis virus, DH-BB (Fig. 4B). The insertion of the ZZ domain into the E2 region (Ohno et al., 1997) and alanine substitutions of the amino acids that affect binding (Morizono et al., 2005) did not completely remove the background infection. This background infection was also maintained even in the case of injection with excess heparan sulfate (data not shown), which has been reported to play a key role in the binding of the Sindbis virus to target cells. It appears that Bergmann glial cells express some unidentified receptors that are involved in this background infection by the Sindbis virus. Further investigations are necessary to improve the specificity of the recombinant Sindbis virus displaying the IgG-binding domain.

In principle, the antibody-displaying viral vector particles can reach the target cells from their extracellular sides. Thus, we used antibodies that bind to the extracellular domains of the membrane proteins. For example, for the *in vitro* assay, we used an antibody that was directed against an extracellular region of the human $p75^{NTR}$, of which 15/16 amino acid residues are identical to those in rats. In the case of the *in vivo* assay, the anti-GFP antibody that was available for immunohistochemistry was used, and the targeted neurons expressed synaptopHluorin, in which a pH-sensitive derivative of GFP (pHluorin) is connected to the lumenal domain of a vesicular membrane protein, VAMP-2 (Miesenböck et al., 1998; Yuste et al., 2000). The pHluorins, which are recognized by the anti-GFP antibody, are expected to face the extracellular space, as a number of VAMP-2 molecules are also distributed in the plasma membrane (Takamori et al., 2006; Walch-Solimena et al., 1995).

The functions of neural cells have been characterized by membrane proteins including channels, transporters and receptors. Some adhesion molecules, such as members of the cadherin family, the integrin family, and the immunoglobulin superfamily, which are expressed in the membrane, are known to play important roles in axon guidance (Goodman, 1996; Maness and Schachner, 2007; Nakamoto et al., 2004; Yu and Bargmann, 2001) and synaptic connections (Takeichi, 2007; Rohrbough et al., 2000). Gene transfer techniques that utilize antibody-displaying viral vectors and the development of various antibodies that target the extracellular domains of membrane proteins could become powerful tools for neuroscience. Although the effectiveness of transfection could be improved by increasing the viral titer, current methods have advantages in labeling a small number of the type-identified cells with high specificity.

5. Conclusions

Here, we showed that ZZ Sindbis can deliver genes with high specificity both *in vitro* and *in vivo*. These data indicate the potential of antibody-displaying viral vectors for transferring a gene to a specific subset of neural cells in the CNS. This result was achieved by selecting an appropriate antibody, although more studies of this

type of viral vector are needed, especially regarding the relationship between the antibodies and targeted neural cells.

Acknowledgements

The authors gratefully thank Dr. Douglas Sipp for his manuscript corrections and Brent Bell for language assistance. This work was sponsored by the Program for Promotion of Fundamental Studies in Health Sciences of the National Institute of Biomedical Innovation (NIBIO), Global COE Program (Basic & Translational Research Centre for Global Brain Science), MEXT and Strategic Research Program for Brain Sciences (SRPBS), MEXT. The funders had no role in study design, data collection and analysis, decision to publish, or preparation of the manuscript.

Appendix A. Supplementary data

Supplementary data associated with this article can be found, in the online version, at doi:10.1016/j.neures.2011.08.013.

References

Araki, R., Sakagami, H., Yanagawa, Y., Hikima, T., Ishizuka, T., Yawo, H., 2005. Transgenic mouse lines expressing synaptopHluorin in hippocampus and cerebellar cortex. Genesis 42, 53–60.

Bredenbeek, P.J., Frolov, I., Rice, C.M., Schlesinger, S., 1993. Sindbis virus expression vectors: packaging of RNA replicons by using defective helper RNAs. J. Virol. 67, 6439–6446.

Chao, M.V., 2003. Neurotrophins and their receptors: a convergence point for many signalling pathways. Nat. Rev. Neurosci. 4 (4), 299–309.

Dechant, G., Barde, Y.-A., 2002. The neurotrophin receptor p75NTR: novel functions and implications for diseases of the nervous system. Nat. Neurosci. 5 (11), 1131–1136.

Frolov, I., Schlesinger, S., 1994. Comparison of the effects of Sindbis virus and Sindbis virus replicons on host cell protein synthesis and cytopathogenicity in BHK cells. J. Virol. 68, 1721–1727.

Garoff, H., Wilschut, J., Liljestrom, P., Wahlberg, J.M., Bron, R., Suomalainen, M., Smyth, J., Salminen, A., Barth, B.U., Zhao, H., et al., 1994. Assembly and entry mechanisms of Semliki Forest virus. Arch. Virol. Suppl. 9, 329–338.

Goodman, C.S., 1996. Mechanisms and molecules that control growth cone guidance. Ann. Rev. Neurosci. 19, 341–377.

Horikawa, H.P.M., Saisu, H., Ishizuka, T., Sekine, Y., Tsugita, A., Odani, S., Abe, T., 1993. A complex of rab3A, SNAP-25 VAMP/synaptobrevin-2 and syntaxins in brain presynaptic terminals. FEBS Lett. 330 (2), 236–240.

Huang, H.V., 1996. Sindbis virus vectors for expression in animal cells. Curr. Opin. Biotechnol. 7, 531–535.

Ishizuka, T., Kakuda, M., Araki, R., Yawo, H., 2006. Kinetic evaluation of photosensitivity in genetically engineered neurons expressing green algae light-gated channels. Neurosci. Res. 54 (2), 85–94.

Kaplan, D.R., Miller, F.D., 2000. Neurotrophin signal transduction in the nervous system. Curr. Opin. Neurobiol. 10 (3), 381–391.

Korokhov, N., Mikheeva, G., Krendelshchikov, A., Belousova, N., Simonenko, V., Krendelshchikova, V., Pereboev, A., Kotov, A., Kotova, O., Triozzi, P.L., Aldrich, W.A., Douglas, J.T., Lo, K.-M., Banerjee, P.T., Gillies, S.D., Curiel, D.T., Krasnykh, V., 2003. Targeting of adenovirus via genetic modification of the viral capsid combined with a protein bridge. J. Virol. 77, 12931–12940.

Maletic-Savatic, M., Malinow, R., Svoboda, K., 1999. Rapid dendritic morphogenesis in CA1 hippocampal dendrites induced by synaptic activity. Science 283, 1923–1927.

Maness, P.F., Schachner, M., 2007. Neural recognition molecules of the immunoglobulin superfamily: signaling transducers of axon guidance and neuronal migration. Nat. Neurosci. 10 (1), 19–26.

Miesenböck, G., De Angelis, D.A., Rothman, J.E., 1998. Visualizing secretion and synaptic transmission with pH-sensitive green fluorescent proteins. Nature 394, 192–195.

Morizono, K., Chen, I.S.Y., 2005. Targeted gene delivery by intravenous injection of retroviral vectors. Cell Cycle 4, 854–856.

Morizono, K., Xie, Y., Ringpis, G.-E., Johnson, M., Nassanian, H., Lee, B., Wu, L., Chen, I.S.Y., 2005. Lentiviral vector retargeting to P-glycoprotein on metastatic melanoma through intravenous injection. Nat. Med. 11, 346–352.

Nagai, T., Ibata, K., Park, E.S., Kubota, M., Mikoshiba, K., Miyawaki, A., 2002. A variant of yellow fluorescent protein with fast and efficient maturation for cell-biological applications. Nat. Biotechnol. 20, 87–90.

Nakamoto, T., Kain, K.H., Ginsberg, M.H., 2004. Neurobiology: new connections between integrins and axon guidance. Curr. Biol. 14 (3), R121–R123.

Nargi-Aizenman, J.L., Griffin, D.E., 2001. Sindbis virus-induced neuronal death is both necrotic and apoptotic and is ameliorated by N-methyl-D-aspartate receptor antagonists. J. Virol. 75, 7114–7121.

Niederhauser, O., Mangold, M., Schubenel, R., Kusznir, E.A., Schmidt, D., Hertel, C., 2000. NGF ligand alters NGF signaling via p75NTR and TrkA. J. Neurosci. Res. 61 (3), 263–272.

Nilsson, B., Moks, T., Jansson, B., Abrahmsen, L., Elmblad, A., Holmgren, E., Henrichson, C., Jones, T.A., Uhlen, M., 1987. A synthetic IgG-binding domain based on staphylococcal protein A. Protein Eng. 1, 107–113.

Ohno, K., Sawai, K., Iijima, Y., Levin, B., Meruelo, D., 1997. Cell-specific targeting of Sindbis virus vectors displaying IgG-binding domains of protein A. Nat. Biotechnol. 15, 763–767.

Portales-Casamar, E., Swanson, D.J., Liu, L., Leeuw, C.N.d., Banks, K.G., Ho Sui, S.J., Fulton, D.L., Ali, J., Amirabbasi, M., Arenillas, D.J., Babyak, N., Black, S.F., Bonaguro, R.J., Brauer, E., Candido, T.R., Castellarin, M., Chen, J., Chen, Y., Cheng, J.C.Y., Chopra, V., Docking, T.R., Dreolini, L., D'Souza, C.A., Flynn, E.K., Glenn, R., Hatakka, K., Hearty, T.G., Imanian, B., Jiang, S., Khorasan-zadeh, S., Komljenovic, I., Laprise, S., Liao, N.Y., Lim, J.S., Lithwick, S., Liu, F., Liu, J., Lu, M., McConechy, M., McLeod, A.J., Milisavljevic, M., Mis, J., O'Connor, K., Palma, B., Palmquist, D.L., Schmouth, J.-F., Swanson, M.I., Tam, B., Ticoll, A., Turner, J.L., Varhol, R., Vermeulen, J., Watkins, R.F., Wilson, G., Wong, B.K.Y., Wong, S.H., Wong, T.Y.T., Yang, G.S., Ypsilanti, A.R., Jones, S.J.M., Holt, R.A., Goldowitz, D., Wasserman, W.W., Simpson, E.M., 2010. A regulatory toolbox of MiniPromoters to drive selective expression in the brain. Proc. Natl. Acad. Sci. U. S. A. 107, 16589–16594.

Ried, M.U., Girod, A., Leike, K., Buning, H., Hallek, M., 2002. Adeno-associated virus capsids displaying immunoglobulin-binding domains permit antibody-mediated vector retargeting to specific cell surface receptors. J. Virol. 76, 4559–4566.

Rohrbough, J., Grotewiel, M.S., Davis, R.L., Broadie, K., 2000. Integrin-mediated regulation of synaptic morphology, transmission, and plasticity. J. Neurosci. 20 (18), 6868–6878.

Sankaranarayanan, S., De Angelis, D., Rothman, J.E., Ryan, T.A., 2000. The use of pHluorins for optical measurements of presynaptic activity. Biophys. J. 79, 2199–2208.

Schaffer, D.V., Koerber, J.T., Lim, K.-i., 2008. Molecular engineering of viral gene delivery vehicles. Ann. Rev. Biomed. Eng. 10, 169–194.

Shaner, N.C., Campbell, R.E., Steinbach, P.A., Giepmans, B.N.G., Palmer, A.E., Tsien, R.Y., 2004. Improved monomeric red, orange and yellow fluorescent proteins derived from Discosoma sp. red fluorescent protein. Nat. Biotechnol. 22, 1567–1572.

Söllner, T., Whiteheart, S.W., Brunner, M., Erdjument-Bromage, H., Geromanos, S., Tempst, P., Rothman, J.E., 1993. SNAP receptors implicated in vesicle targeting and fusion. Nature 362 (6418), 318–324.

Tai, C.-K., Logg, C.R., Park, J.M., Anderson, W.F., Press, M.F., Kasahara, N., 2003. Antibody-mediated targeting of replication-competent retroviral vectors. Hum. Gene Ther. 14, 789–802.

Takamori, S., Holt, M., Stenius, K., Lemke, E.A., Grønborg, M., Riedel, D., Urlaub, H., Schenck, S., Brügger, B., Ringler, P., Müller, S.A., Rammner, B., Gräter, F., Hub, J.S., De Groot, B.L., Mieskes, G., Moriyama, Y., Klingauf, J., Grubmüller, H., Heuser, J., Wieland, F., Jahn, R., 2006. Molecular anatomy of a trafficking organelle. Cell 127, 831–846.

Takeichi, M., 2007. The cadherin superfamily in neuronal connections and interactions. Nat. Rev. Neurosci. 8 (1), 11–20.

Waehler, R., Russell, S.J., Curiel, D.T., 2007. Engineering targeted viral vectors for gene therapy. Nat. Rev. Genet. 8, 573–587.

Walch-Solimena, C., Blasi, J., Edelmann, L., Chapman, E.R., von Mollard, G.F., Jahn, R., 1995. The t-SNAREs syntaxin 1 and SNAP-25 are present on organelles that participate in synaptic vesicle recycling. J. Cell Biol. 128, 637–645.

Yu, T.W., Bargmann, C.I., 2001. Dynamic regulation of axon guidance. Nat. Neurosci. 4, 1169–1176.

Yuste, R., Miller, R.B., Holthoff, K., Zhang, S., Miesenböck, G., 2000. Synapto-pHluorins: chimeras between pH-sensitive mutants of green fluorescent protein and synaptic vesicle membrane proteins as reporters of neurotransmitter release. Methods Enzymol. 327, 522–546.

ARTICLE

BIOTECHNOLOGY AND BIOENGINEERING

Optically Controlled Contraction of Photosensitive Skeletal Muscle Cells

Toshifumi Asano,[1,2] Toru Ishizua,[1,3] Hiromu Yawo[1,3,4,5]

[1]Department of Developmental Biology and Neuroscience, Tohoku University Graduate School of Life Sciences, Sendai, Japan; telephone: +81-22-217-6208; fax: +81-22-217-6211; e-mail: yawo-hiromu@m.tohoku.ac.jp

[2]Japan Society for the Promotion of Science, Chiyoda, Tokyo, Japan

[3]Japan Science and Technology Agency (JST), Core Research of Evolutional Science & Technology (CREST), Tokyo, Japan

[4]Tohoku University Basic and Translational Research Center for Global Brain Science, Sendai, Japan

[5]Center for Neuroscience, Tohoku University Graduate School of Medicine, Sendai, Japan

Received 19 April 2011; revision received 8 July 2011; accepted 25 July 2011

Published online 1 August 2011 in Wiley Online Library (wileyonlinelibrary.com). DOI 10.1002/bit.23285

ABSTRACT: As the skeletal muscle cell is an efficient force transducer, it has been incorporated in bio-microdevices using electrical field stimulation for generating contractile patterns. To improve both the spatial and temporal resolutions, we made photosensitive skeletal muscle cells from murine C2C12 myoblasts, which express channelrhodopsin-2 (ChR2), one of archaea-type rhodopsins derived from green algae *Chlamydomonas reinhardtii*. The cloned ChR2-expressing C2C12 myoblasts were made and fused with untransfected C2C12 to form multinucleated myotubes. The maturation of myotubes was facilitated by electrical field stimulation. Blue LED light pulse depolarized the membrane potential of a ChR2-expressing myotube and eventually evoked an action potential. It also induced a twitch-like contraction in a concurrent manner. A contraction pattern was thus made with a given pattern of LED pulses. This technique would have many applications in the bioengineering field, such as wireless drive of muscle-powered actuators/microdevices.

Biotechnol. Bioeng. 2012;109: 199–204.

KEYWORDS: optical stimulation; channelrhodopsin; C2C12; myotube; myoblast; muscle contraction

Introduction

Bio-microdevices incorporating biological components such as tissues, cells, and biomolecules have raised much attention for the development of novel engineering devices. Muscle cells could provide force-generating modules driven by the activation of actin–myosin motors coordinated with excitation–contraction coupling (Bers, 2002). As an efficient force transducer, a muscle-powered micro-actuator driven by biochemical energy reaction could save energy, resources, and space. With these advantages, contractile muscles have been incorporated into engineered bio-microdevices to create motors, actuators (Feinberg et al., 2007; Kim et al., 2007; Morishima et al., 2006; Wilson et al., 2010; Xi et al., 2005), and pumps (Tanaka et al., 2007). Conventionally, muscle contraction has been triggered by electrical field stimulation using electrodes placed in the extracellular space. Alternatively, spontaneously beating cardiac muscle cells have also been used. Electrical field stimulation is a simple method to control the temporal pattern of contractile activity. However, the electrical field is generally non-uniform and many unexpected muscle cells are stimulated simultaneously. It is thus difficult to specifically stimulate identified groups of muscle cells.

The optical stimulation methods have raised much attention recently because of their advantages over conventional electrical stimulation methods: Fine resolution in space and time, parallel stimulations at multiple sites, relative harmlessness and convenience (Callaway and Yuste, 2002; Miesenböck, 2004). Recently, photostimulation using channelrhodopsin-2 (ChR2), which are involved in the light-dependent behavior of a unicellular green alga, *Chlamydomonas reinhardtii* (Nagel et al., 2003), has become a powerful tool for the investigation of neural networks in vivo and in vitro (Boyden et al., 2005; Ishizuka et al., 2006; Li et al., 2005).

In this study, to render contractile muscle photosensitive, one of the mouse muscle sarcoma cell lines, C2C12 myoblast

Correspondence to: H. Yawo

Contract grant sponsor: Ministry of Education, Culture, Sports, Science and Technology (MEXT) of Japan

Additional supporting information may be found in the online version of this article

(Yaffe and Saxel, 1977), is genetically engineered to express ChR2. The C2C12 myoblasts are fused with each other in vitro, becoming contractile with the formation of myofibrils, and are applied to study skeletal muscle cell physiology (Fujita et al., 2007; Nakanishi et al., 2007; Nedachi and Kanzaki, 2006; Yamaguchi et al., 2010) or contractive mechanics (Kaji et al., 2010; Nagamine et al., 2011; Yamasaki et al., 2009). We found that patterned contraction of ChR2-expressing myotubes was robustly triggered by blue LED light. Optical stimulation techniques with the combination of ChR2-expressing C2C12 myoblasts and microfabrication could enable wireless manipulation of muscle-powered actuators/microdevices.

Materials and Methods

Cell Culture and Generation of ChR2-Venus-Transfected C2C12 Cell Lines

Murine C2C12 myoblasts were obtained from RIKEN Cell Bank (RCB0987) and cultured at 37°C under a 5% CO_2 atmosphere in Dulbecco's Modified Eagle's Medium (DMEM, Sigma–Aldrich, St. Louis, MO) supplemented with 10% Fetal Bovine Serum (FBS, Biological Industries Ltd), 100 units/mL penicillin, 100 μg/mL streptomycin (Sigma–Aldrich). A murine leukemia virus-based vector, SRα-chop2-Venus, was constructed by replacing enhanced green fluorescent protein (EGFP) in SRαLEGFP with ChR2 apoprotein tagged with a modified yellow fluorescent protein, Venus (Nagai et al., 2002), and the pseudovirions were prepared as described previously (Kamada et al., 2004). The titer of the virus stock was 1.4×10^5 infectious particles per mL. To generate ChR2-Venus expressing stable lines, C2C12 cells were transfected with the virions and cloned twice by limited dilution. Single-cell clones with bright Venus fluorescence were selected under the conventional inverted-fluorescent microscopy.

Formation and Maturation of Myotubes

Once confluent, the C2C12 myoblasts were induced to differentiate into myotubes in the differentiation medium consisting of DMEM supplemented with 2% calf serum (Thermo Fisher Scientific, Waltham, MA), 1 nM insulin (Invitrogen, Carlsbad CA), 100 units/mL penicillin, and 100 μg/mL streptomycin, which was replaced every 24 h. To facilitate the maturation of myotubes, they were transferred to electrical field stimulation medium, which was composed of DMEM supplemented with 2% calf serum, 2% MEM amino acid solution (Invitrogen), 1% MEM non-essential amino acid solution (Invitrogen), 100 units/mL penicillin, and 100 μg/mL streptomycin. Electrical pulses (0.8 V/mm, 2 ms duration) were generated by a pulse generator (SEN-7203, Nihon Kohden, Tokyo, Japan) and applied at 1 Hz continuously for 3 days through bipolar carbon electrode plates. The electrical field stimulation medium was changed every 12 h during each stimulation protocol.

Electrophysiology

Fluorescence-labeled myotubes were identified under conventional epi-fluorescence microscopy (BH2-RFC, Olympus, Tokyo, Japan) equipped with a 60× water-immersion objective (LUMplanPl/IR60x, Olympus). The photocurrents were recorded as described previously (Ishizuka et al., 2006) under the whole-cell patch clamp of a conventional system (Axopatch 200A plus Digidata1200, Molecular Devices Co.). The standard patch pipette solution contained (in mM): 40 KCl, 80 KCH_3SO_4, 10 HEPES, 1 $MgCl_2$, 2.5 MgATP, 0.2 Na_2EGTA (pH 7.4 adjusted with KOH). The standard extracellular solution contained (in mM): 138 NaCl, 3 KCl, 1 $CaCl_2$, 1 $MgCl_2$, 10 HEPES, 4 NaOH (pH 7.4 adjusted with HCl). All the experiments were carried out at room temperature.

Immunocytochemistry

The cultured myotubes were washed with PBS and fixed for 15 min in 0.1 M PBS (pH 7.4) containing 4% paraformaldehyde (PFA) and 0.1% Triton X-100. The specimens were blocked in PBS with 5% donkey serum for 1 h and reacted with mouse monoclonal anti-sarcomeric α-actinin primary antibody (1:400; Sigma–Aldrich) in PBS with 5% donkey serum and 0.1% Triton X-100 for 1 h. After washing three times in PBS with 0.1% Triton X-100, the cells were incubated for 1–2 h with the Alexa Fluor 546-conjugated anti-mouse IgG secondary antibody in PBS with 5% donkey serum and 0.1% Triton X-100. Alexa Fluor 633-labeled phalloidin was added to the secondary antibody solution to visualize the filamentous actin (F-actin). All of the above reactions were done at room temperature. The specimens were mounted with Vectashield (Vector Laboratories, Burlingame, CA) and coverslipped. The fluorescent images were taken under conventional confocal laser microscopy (LSM510META, Carl Zeiss, Oberkochen, Germany) equipped with a 40× objective and corrected for brightness and contrast using conventional software (LSM Image Browser).

Optical Stimulation and Motion Analysis

Optical stimulation was carried out by blue LED (470 ± 25 nm, LXHL-NB98, Philips Lumileds Lighting Inc. San Jose, CA) regulated by a pulse generator (SEN-7203, Nihon Kohden) with a current booster (SEG-3104, Nihon Kohden) in a high-calcium extracellular solution (in mM, 138 NaCl, 3 KCl, 10 HEPES, 4 NaOH, 1.25 $MgCl_2$, 10 $CaCl_2$, pH 7.4 adjusted with HCl). Its light power density was directly measured by a thermopile (MIR-100Q, Mitsubishi Oil Chemicals, Tokyo, Japan) and was 0.12

mW/mm^2 at the bottom of the culture dish. Each photostimulation protocol was given with an interval of 3–5 min. The contractile movements of myotubes were monitored by a CCD camera (VB-7010, Keyence Co., Osaka, Japan; 7.5 frames/s) under phase-contrast microscopy. Each sequential image was converted to gray scale, inverted in brightness, and the point of maximal pixel value was identified in the region of interest covering the myotube. The contractile displacement was measured by tracking this point, and expressed in μm after correcting the scale. All the above image analyses were carried out using ImageJ software (NIH, Bethesda, MD).

Results and Discussions

Formation of C2C12 Myotubes Expressing ChR2

Probably due to repeated passage before establishing the cloned myoblasts which stably express ChR2 (ChR2-C2C12), they did not form well-differentiated myotubes. Since the C2C12 cells fused with each other and formed multi-nucleated myotubes (Blau et al., 1983), this genetic deficit was expected to be overcome by fusion with untransfected C2C12 (UT-C2C12) cells. Therefore, we co-cultured ChR2-C2C12 cells with UT-C2C12 cells in the ratio of 1:2 and rendered them to be fused with each other. As shown in Fig. 1A the multi-nucleated myotubes expressing ChR2-Venus were almost similar to those from UT-C2C12 cells in gross appearance. Under confocal microscopy, ChR2-Venus was distributed uniformly at the contour of the multi-nucleated myotube, suggesting that it was localized in the plasma membrane (Fig. 1B). Among multi-nucleated myotubes, about 80% were expressed ChR2-Venus. Therefore, the ChR2-C2C12 cells appear to be fused with the UT-C2C12 cells to form multi-nucleated myotubes with the diffusion of ChR2-Venus molecules along their plasma membranes.

Photocurrents were evoked by 100 ms blue LED light pulses of variable strength under whole-cell patch clamp of the multi-nucleated myotube expressing ChR2-Venus (Fig. 2A). The blue LED light induced a negative current with a peak and a plateau at a holding potential of −60 mV, as reported previously (Ishizuka et al., 2006). Both the peak and plateau currents were dependent on the light intensity. Under current-clamp, the resting potential was between −50 and −30 mV (n = 7) and action potentials were not evoked even by direct current injection. When hyperpolarized to around −70 mV, the blue LED light pulse evoked membrane depolarization and, eventually, an action potential similar to that by the direct current injection (Fig. 2B). However, the light-evoked action potential frequently failed to be evoked even at the maximal strength (0.08 mW/mm^2) and no action potential was evoked in two myotubes. In another two myotubes, each depolarization, either electrically or optically, was sometimes accompanied with contraction, but frequently was not.

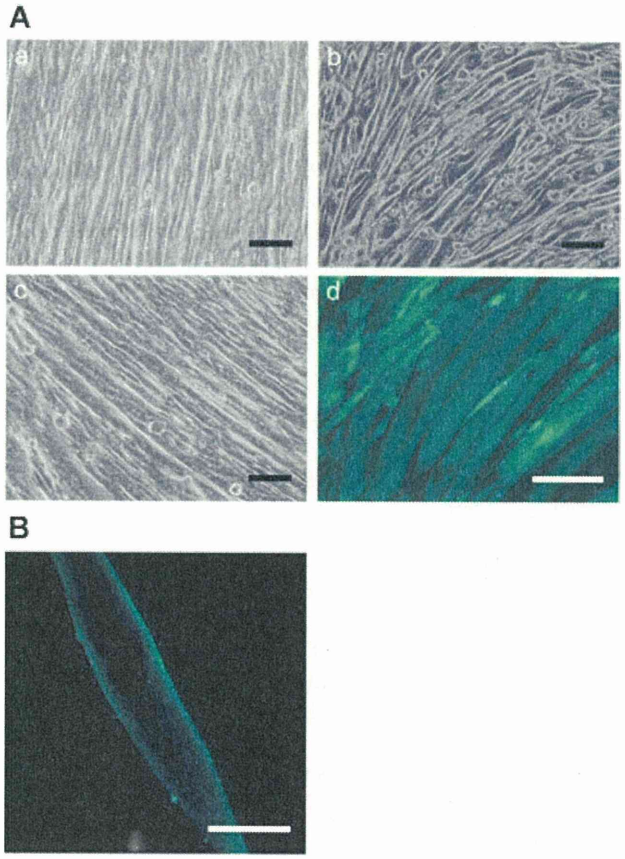

Figure 1. ChR2-expressing C2C12 myotubes. **A**: Phase-contrast images of multinucleated myotubes cultured in the differentiation medium for 10 days; (**a**) from untransfected (UT)-C2C12, (**b**) from C2C12 cells which stably expressed ChR2 (ChR2-C2C12), (**c**) from co-cultured ChR2-C2C12 with UT-C2C12 in the ratio of 1:2 and (**d**) Venus-fluorescence images of co-cultured myotubes. Note that some of them expressed ChR2-Venus conjugates. **B**: A confocal image of typical multi-nucleated myotubes expressing ChR2-Venus conjugates. Scale bars: 100 μm in A, 20 μm in B. [Color figure can be seen in the online version of this article, available at http://wileyonlinelibrary.com/bit]

Maturation of Myotubes

Under conventional differentiation conditions, the development of sarcomere structure in a C2C12 myotube is very slow and its contractile activity is also retarded (Engler et al., 2004). However, it has been reported that the electrical field stimulation evoked membrane depolarization, transiently increased the intracellular Ca^{2+}, accelerated the sarcomere assembly, and facilitated the contractile activity in the C2C12 myotube (Fujita et al., 2007). Before applying the electrical field stimulation protocol, the sarcomeric structure, which is the smallest contractile unit, was not obvious in the C2C12 myotubes (Fig. 3A). On the other hand, after 3-day application of the electrical field stimulation protocol (0.8 V/mm, 2 ms pulse at 1 Hz), which was given by electrodes placed in the culture dish, striation patterns consisting of sarcomeric α-actinin and F-actin were manifest in the C2C12 myotubes (Fig. 3B). The sarcomeric

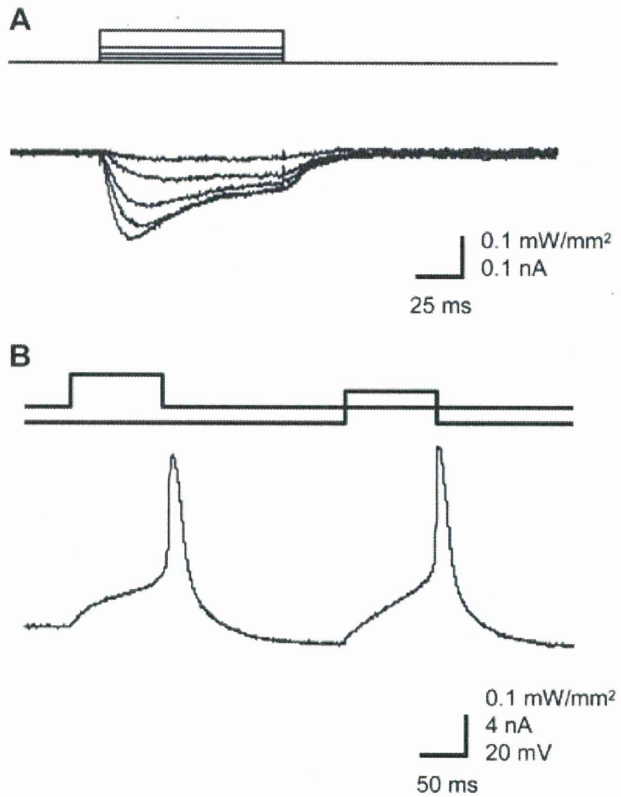

Figure 2. Optical stimulation of ChR2-expressing C2C12 myotube. **A**: Top, blue LED light pulses and bottom, photocurrent responses of a multi-nucleated myotube from ChR2-C2C12 co-cultured with UT-C2C12. **B**: Top, blue LED light pulse, middle, current injection from the patch electrode, and bottom, a typical membrane potential response. Resting potential, −67 mV.

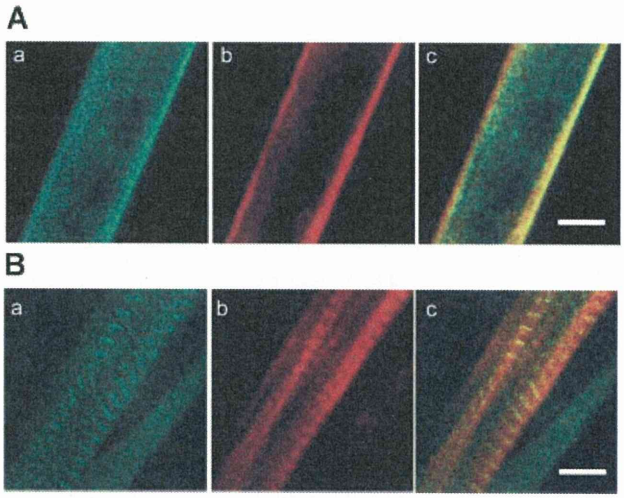

Figure 3. Maturation of sarcomeric structures. **A**: The ChR2-expressing C2C12 myotube before applying the electrical field stimulation protocol. **a**: Distribution of anti-α-actinin immunoreactivity (green). **b**: Distribution of F-actin indicated by Alexa Fluor 633-labeled phalloidin. **c**: Merged image of (a) and (b). **B**: The maturated myotube after 3-day application of electrical filed stimulation protocol with similar panels (**a**)–(**c**) as in (A). Scale bars: 10 μm.

structure appeared to be prominently localized in a banded pattern which ran in a longitudinal direction along each myotube. These results were consistent with those of previous studies (Fujita et al., 2007; Nagamine et al., 2010), and the periodic electrical stimulation efficiently facilitated the assembly of sarcomeric structures.

Contractile Activity Controlled by Optical Stimulation

After 3-day electrical field stimulation, the contractile activity of the ChR2-Venus-expressing myotubes was examined using optical stimulation by blue LED (0.12 mW/mm^2, 100 ms duration) and electrical field stimulation (0.8 V/mm, 100 ms duration). Typically, these myotubes showed obvious contraction synchronous to each light or electric pulse of a given frequency (Supplementary Movie S1–8). As shown in Fig. 4A, the myotube twitched almost concurrently with every light or electric pulse at frequencies between 1 and 4 Hz. However, the response to 5 Hz stimulation varied from one myotube to another. In the case shown in Fig. 4A, the contraction was attenuated by light or electric pulses given in the later period (Supplementary Movie S9, 10). Otherwise, the myotube twitched robustly at 5 Hz (Fig. 4B and Supplementary Movie S11, 12) or exhibited tetanus-like sustained contraction (Fig. 4C and Supplementary Movie S13, 14) during either optical or electrical stimulation. The optically evoked contractions were almost similar to the electrically evoked ones in both the contractile pattern and the magnitude as indicated by the average contraction lengths during the stimulation period (Fig. 4D). Therefore, the various contractile patterns at high-frequency stimulation could be attributed to the various maturational levels of the myotubes. In some myotubes, the optical stimulation evoked no contractions at the maximal light intensity, probably because of the low expression level of ChR2.

Muscle fibers in vivo have been subjected contractile activity under the regulation of nerve-muscle synapses. However, it has been difficult to engineer neuro-muscular synapses in vitro to manipulate microdevices with desired accuracy. Hitherto, electrical field stimulation has been mainly used for artificial contraction of skeletal muscles. However, it has several disadvantages such as low point-to-point discrimination, electrolysis of electrodes, and tissue damage. In contrast, optical methods allow one to stimulate muscle cells without any contact with tissue or extracellular fluid, and thus are non-invasive in principle. Since the optical signal is also high in both spatial and temporal resolutions, it should enable one to control the muscle contraction accurately with given spatial and temporal patterns, which has never been achieved by electrical stimulation.

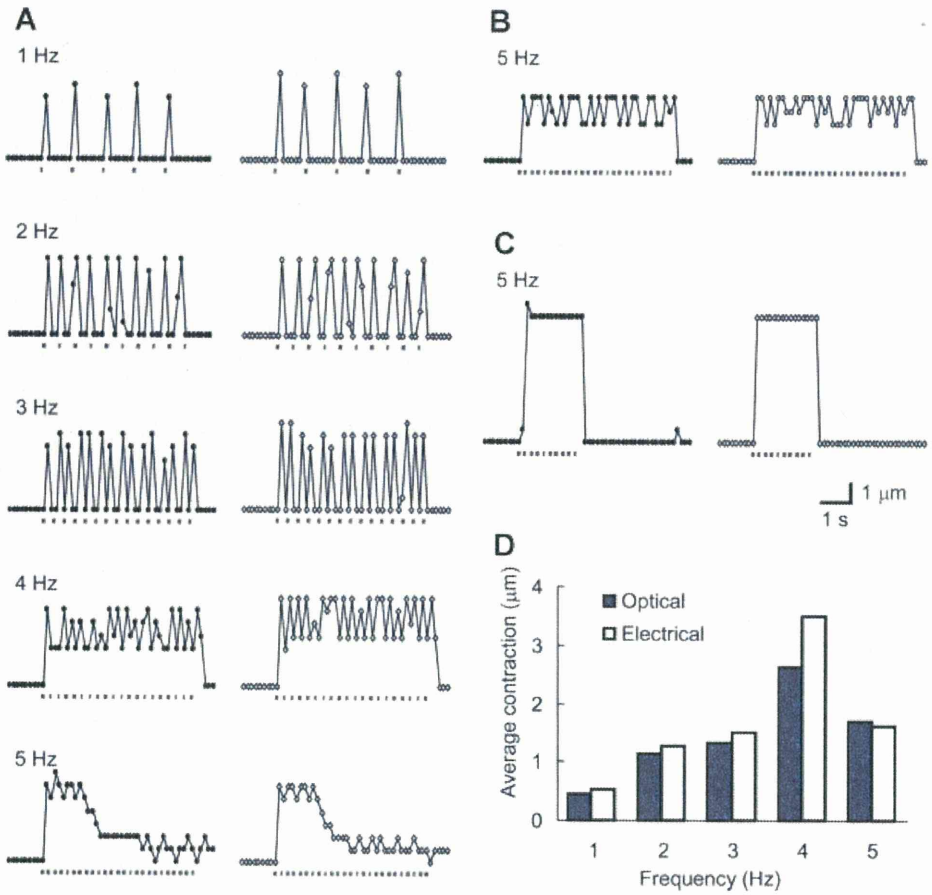

Figure 4. Optically evoked contraction of ChR2-expressing C2C12 myotube. **A**: Typical contraction patterns of a myotube during a 5-s train of LED pulses (0.12 mW/mm^2, 100 ms duration) each at 1, 2, 3, 4, and 5 Hz (from top to bottom of the left column) or during electrical field stimulation (0.8 V/mm, 100 ms duration, right column). **B**: Pulse-to-pulse contraction of another myotube at 5 Hz. **C**: An example of tetanus-like contraction evoked by 5 Hz photostimulation. **D**: Average contraction length during the stimulation period of 5 s of a ChR2-expressing myotube in response to either optical or electrical field stimuli. From the same myotube shown in A. The same scales for A–C.

Conclusions

In this paper it was shown that the C2C12 myotubes became photosensitive by the expression of one of the light-gated channels, ChR2, and that optical stimulation using LED light pulses was able to control their contractile activity with a given temporal pattern. This technique would have many potential bioengineering applications such as wireless drive of muscle-powered actuators/microdevices and aneural culture model systems that may be used for the study of muscle fiber maturation, muscle bioassays for biological and mechanical properties, and pathophysiological study of muscular dystrophy. With the development of ES/iPS-cell technologies, the present methods would enable one to generate human muscle tissue substitutes the contraction of which is optically regulated.

The authors are grateful to K. Nagamine and M. Kanzaki for technical advices and to B. Bell and D. Teh for language assistance. This work was supported by grant-in-aid for Japan Society for the Promotion of Science (JSPS) Fellows, Core Research for Evolutional Science and Technology (CREST), Japan Science and Technology Agency (JST) and grants-in-aid for scientific research from the Ministry of Education, Culture, Sports, Science and Technology (MEXT) of Japan.

References

Bers DM. 2002. Cardiac excitation-contraction coupling. Nature 415(6868): 198–205.

Blau HM, Chiu C-P, Webster C. 1983. Cytoplasmic activation of human nuclear genes in stable heterocaryons. Cell 32(4):1171–1180.

Boyden ES, Zhang F, Bamberg E, Nagel G, Deisseroth K. 2005. Millisecond-timescale, genetically targeted optical control of neural activity. Nat Neurosci 8(9):1263–1268.

Callaway EM, Yuste R. 2002. Stimulating neurons with light. Curr Opin Neurobiol 12(5):587–592.

Engler AJ, Griffin MA, Sen S, Bonnetnann CG, Sweeney HL, Discher DE. 2004. Myotubes differentiate optimally on substrates with tissue-like stiffness: Pathological implications for soft or stiff microenvironments. J Cell Biol 166(6):877–887.

Feinberg AW, Feigel A, Shevkoplyas SS, Sheehy S, Whitesides GM, Parker KK. 2007. Muscular thin films for building actuators and powering devices. Science 317(5843):1366–1370.

Fujita H, Nedachi T, Kanzaki M. 2007. Accelerated de novo sarcomere assembly by electric pulse stimulation in C2C12 myotubes. Exp Cell Res 313(9):1853–1865.

Ishizuka T, Kakuda M, Araki R, Yawo H. 2006. Kinetic evaluation of photosensitivity in genetically engineered neurons expressing green algae light-gated channels. Neurosci Res 54(2):85–94.

Kaji H, Ishibashi T, Nagamine K, Kanzaki M, Nishizawa M. 2010. Electrically induced contraction of C2C12 myotubes cultured on a porous membrane-based substrate with muscle tissue-like stiffness. Biomaterials 31(27):6981–6986.

Kamada M, Li RY, Hashimoto M, Kakuda M, Okada H, Koyanagi Y, Ishizuka T, Yawo H. 2004. Intrinsic and spontaneous neurogenesis in the postnatal slice culture of rat hippocampus. Eur J Neurosci 20(10): 2499–2508.

Kim J, Park J, Yang S, Baek J, Kim B, Lee SH, Yoon E-S, Chun K, Park S. 2007. Establishment of a fabrication method for a long-term actuated hybrid cell robot. Lab Chip 7(11):1504–1508.

Li X, Gutierrez DV, Hanson MG, Han J, Mark MD, Chiel H, Hegemann P, Landmesser LT, Herlitze S. 2005. Fast noninvasive activation and inhibition of neural and network activity by vertebrate rhodopsin and green algae channelrhodopsin. Proc Natl Acad Sci USA 102(49): 17816–17821.

Miesenböck G. 2004. Genetic methods for illuminating the function of neural circuits. Curr Opin Neurobiol 14(3):395–402.

Morishima K, Tanaka Y, Ebara M, Shimizu T, Kikuchi A, Yamato M, Okano T, Kitamori T. 2006. Demonstration of a bio-microactuator powered by cultured cardiomyocytes coupled to hydrogel micropillars. Sens Act B Chem 119(1):345–350.

Nagai T, Ibata K, Park ES, Kubota M, Mikoshiba K, Miyawaki A. 2002. A variant of yellow fluorescent protein with fast and efficient maturation for cell-biological applications. Nat Biotechnol 20(1):87–90.

Nagamine K, Kawashima T, Ishibashi T, Kaji H, Kanzaki M, Nishizawa M. 2010. Micropatterning contractile C2C12 myotubes embedded in a fibrin gel. Biotechnol Bioeng 105(6):1161–1167.

Nagamine K, Kawashima T, Sekine S, Ido Y, Kanzaki M, Nishizawa M. 2011. Spatiotemporally controlled contraction of micropatterned skeletal muscle cells on a hydrogel sheet. Lab Chip 11(3):513–517.

Nagel G, Szellas T, Huhn W, Kateriya S, Adeishvili N, Berthold P, Ollig D, Hegemann P, Bamberg E. 2003. Channelrhodopsin-2, a directly light-gated cation-selective membrane channel. Proc Natl Acad Sci USA 100(24):13940–13945.

Nakanishi K, Dohmae N, Morishima N. 2007. Endoplasmic reticulum stress increases myofiber formation in vitro. FASEB J 21(11):2994–3003.

Nedachi T, Kanzaki M. 2006. Regulation of glucose transporters by insulin and extracellular glucose in C2C12 myotubes. Am J Physiol Endocrinol Metab 291(4):E817–828.

Tanaka Y, Sato K, Shimizu T, Yamato M, Okano T, Kitamori T. 2007. A micro-spherical heart pump powered by cultured cardiomyocytes. Lab Chip 7(2):207–212.

Wilson K, Das M, Wahl KJ, Colton RJ, Hickman J. 2010. Measurement of contractile stress generated by cultured rat muscle on silicon cantilevers for toxin detection and muscle performance enhancement. Plos One 5(6):e11042.

Xi J, Schmidt JJ, Montemagno CD. 2005. Self-assembled microdevices driven by muscle. Nat Mater 4(2):180–184.

Yaffe D, Saxel ORA. 1977. Serial passaging and differentiation of myogenic cells isolated from dystrophic mouse muscle. Nature 270(5639):725–727.

Yamaguchi T, Suzuki T, Arai H, Tanabe S, Atomi Y. 2010. Continuous mild heat stress induces differentiation of mammalian myoblasts, shifting fiber type from fast to slow. Am J Physiol Cell Physiol 298(1):C140–C148.

Yamasaki K, Hayashi H, Nishiyama K, Kobayashi H, Uto S, Kondo H, Hashimoto S, Fujisato T. 2009. Control of myotube contraction using electrical pulse stimulation for bio-actuator. J Artif Organs 12(2):131–137.